Numerical modeling for seismic microzonation in Singapore

Shynggys Abdialim, B. Eng

Submitted in fulfillment of the requirements
for the degree of Master of Science
in Civil & Environmental Engineering

School of Engineering and Digital Sciences
Department of Civil & Environmental Engineering
Nazarbayev University

53 Kabanbay Batyr Avenue,
Nur-Sultan, Kazakhstan, 010000

Supervisors:

Lead Supervisor: Professor Sung-Woo Moon

Co-Supervisor: Professor Jong Kim

Date of completion: 3 May 2022

DECLARATION

I hereby, declare that this manuscript, 2D and 3D numerical modeling for seismic microzonation in Singapore, is the result of my own work except for quotations and citations which have been duly acknowledged. I also declare that, to the best of my knowledge and belief, it has not been previously or concurrently submitted, in whole or in part, for any other degree or diploma at Nazarbayev University or any other national or international institution.

Name: Shynggys Abdialim

Date: 5/3/2022

Abstract

Dynamic soil property estimation is of crucial step in structural, earthquake design. This is because such soil properties are required in building codes for sustaining lateral dynamic loads adequately, or can be used for evaluation of site specific dynamic phenomena like site amplification, liquefaction. Shear wave velocity can be estimated directly using small strain lab tests (e.g. bender element) or indirectly from geotechnical tests like Standard Penetration test (SPT). Despite having a different test method there is no uniform method that will have a high resolution, be beneficial in terms of time and cost, etc. However, geophysical tests are prone to be advantageous over invasive tests in terms of cost, time and for some cases resolution. This thesis work focuses on an estimation of S-wave velocity using fast and cheap geophysical three component test recordings combined with extra borehole information. Results of such methodology is compared with reference data and application in seismic site classification is demonstrated. Horizontal signal amplification in Bukit Timah Granite territory was assessed using earthquake catalogue, and three seismic stations of Singapore. It is seen that soft sediment in Bukit Timah is prone to horizontal amplification of vibration. Once then numerical modelling of Bukit Timah Granite territory was conducted for assessing the ground shaking phenomenon. For now, it has been demonstrated that the numerical model reveals an adequate simulation results in terms of HVSR results among simulation territory and in comparison with real HVSR data.

Table of Contents

List of Figures

List of tables

Chapter 1. Introduction

1.1. General

With an increase in computational speed of hardware, geophysical site investigation methods which has more than 30-40 years history [1, 2], becoming more and more popular in estimation of shear wave velocity of the soil. Along with that surface wave methods are used for identification of other dynamic soil properties as well: despite the mechanism not being fully researched, Horizontal to Vertical Spectral Ratio (HVSR) is commonly utilized for estimation of fundamental frequency of soft sediment soil layer [3]. Their main advantage over high strain field tests is that surface wave methods are non-invasive and does not require borehole digging. This in turn makes surface wave methods cheaper and faster in covering large areas. Based on number of geophones, noise recording equipment, there are different types of tests even among surface wave tests like single station method (HVSR) and array methods (e.g., active and passive Multichannel Analysis of Surface Waves (MASW)). Especially in highly urbanized territories like Singapore non-invasive and portable nature of test method makes it quite handy [4]. Commonly HVSR method is utilized for estimation of fundamental frequency of the site and HVSR amplitude, which correlation to site amplification factor is quite doubtful. Ellipticity curve inversion is another method of S-wave velocity estimation from HVSR data, but it is highly criticized due to the potential uncertainties.

In this work ellipticity curve inversion method will be conducted; and to increase the certainty of the results additional data taken from borehole logs will be used during the inversion process. Along with that it will be shown that Bukit Timah Granite might have a high horizontal vibration amplification. Thus, numerical modelling will be conducted to assess site effects against dynamic loadings.

1.2. Aims and Objectives

This work aims to ellipticity curve inversion with borehole log information method. It is done for validating the hypothesis stating that in urban areas, where there might be problematic to conduct invasive test, and even non-invasive surface array methods, if borehole near previous borehole log information would be available, inverted profile will show the results with adequate resolution enough for site classification works. Presence of borehole logs near the test site drastically limits the potential testing locations, however it is assumed that in urbanized zones such problems will not commonly occur. Also as a future work using the other

type of geotechnical data for combined inversion or restriction of parameter-space can be examined.

As a next step, this work aims to generate 3D Geomodel of Bukit Timah Territory of Singapore for further site effects analysis and even microtremor works. For now, the work is in progress and 2D soil profiles are being validated with available HVSR data.

1.3. Methodologies and techniques

During the thesis work seismic site characterization test results like HVSR and MASW will be utilized for estimation of shear wave (S-wave) velocity profiles, which in turn will be used for seismic site classification. This task will be achieved by conducting Rayleigh wave ellipticity curve inversion with usage of borehole logs as an additional parameter space restricting data. Originally it was planned to conduct microzonation works based on the results of HVSR test in terms of mapping of soft soil's fundamental frequency map and HVSR peak amplitude map. However, it has been clear that available data is not spread homogeneously among a certain area for conducting such works. Thus, 3D Geomodel based on borehole logs, geophysical test results and geological maps will be generated using LeapFrog software for further analysis in UDEC software. Models assessed using input signals or real earthquake data will be used for geomodel validation via comparison of acceleration-time-histories and further Standard Spectral Ratio.

1.4. Thesis structure

Thesis work will first present the literature review at Chapter 2, providing an information on the methodologies utilized during this and other research programs. Starting from the fundamental concepts of wave propagation and dynamic soil properties and following by the microtremor techniques, its inversion followed by the site classification. Moreover, numerical modelling practices and its aims will be briefly explained following by seismic microzonation concepts. In Chapter 3, results for site classification will be presented. The chapter references to the methodologies and techniques like HVSR and ellipticity curve inversion, details of which are described in Chapter 2, literature review. Chapter 4 describes current results for numerical modeling, followed by technical aspects like software used and current results produced. Modeled SSR and real HVSR data will be compared for assessing the credibility of the models. Chapter 5 will conclude the thesis work by highlighting key aspects and further research plans and potentials of the thesis work.

Chapter 2. Literature review

2.1. Seismic waves

2.1.1. Body waves

Seismic waves are classified into two categories: body waves and surface waves. When it comes to the wave travelling, for the distances till two wavelength there is a clear domination of body waves in wave composition. However, for waves travelling further from its shot location surface waves contributes to the most of energy transformation. The reason is a geometric attenuation effect for beforementioned waves: geometric attenuation for the body waves are the function of inverse of a distance $1/r$; at the same time surface waves are attenuated with a distance's power of $1/\sqrt{r}$. Thus as further the wave travels through the wavefield, the less and less body waves' energy contribution will be. [5, 6].

Based on a wave propagation pattern, body waves are divided into two categories: it is Compression waves (P-waves) and Shear waves (S-waves). Compression waves are also called primary waves due to its highest travel speed through different media. The motion of P-wave is traverses in the same direction as a wave propagation direction and shown in. S-waves in turn travels in a parallel direction to the wave propagation Figure 2.1. Based on its motion, S-waves are further divided into vertical and horizontal S-waves (SV and SH respectively).

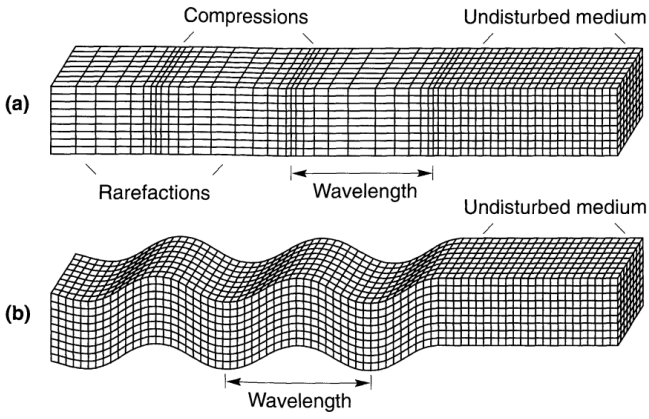

Figure 2.1. Body wave particle motion in (a) P-wave, (b) S-wave [6]

Body waves are non-dispersive, meaning that their velocity will not depend on a frequency component of the wave and will only depend on a geotechnical properties of the soil that it traverses. Both types of the body waves can be expressed by a linear elastic medium properties by the next equations [7, 8]:

$$V_s = \sqrt{(\lambda + 2G)/\rho}$$

$$V_p = \sqrt{G/\rho}$$

Where Vp and Vs are compression and shear wave velocities, respectively. λ – Lame constant, ρ – soil density and G is shear modulus. One other thing to notice that for a non-invasive tests strain level is usually very small, and thus the assumption that there is no need to consider reduction of stiffness properties by strain will be always valid for those equations.

2.1.2. Surface waves

The next type of seismic waves are the surface waves that travels in the upper free surface of the soil and through the boundary of different soil layers. There are two types of surface waves called Rayleigh waves and Love waves. Those waves are usually generated due to the crossing and further interaction of a body waves through the soil boundary mediums[6]. Rayleigh waves are generated via SV and P waves traversed through a soil layer border. The wave itself traverses with an elliptical motion. Due to the easiness of wave generation, Rayleigh wave is commonly used in a geophysical surface wave site tests. Love wave in turn is generated via P and horizontal S-waves. Love wave particle motion is perpendicular to the wave propagation direction. Love wave particle motion can be seen from the Fig. 2.2. It is not commonly used for a site investigation tests due to the complexity of Love wave generation. However, there are still utilized for that purpose and number of researches focused for assessing its applicability are increasing [9].

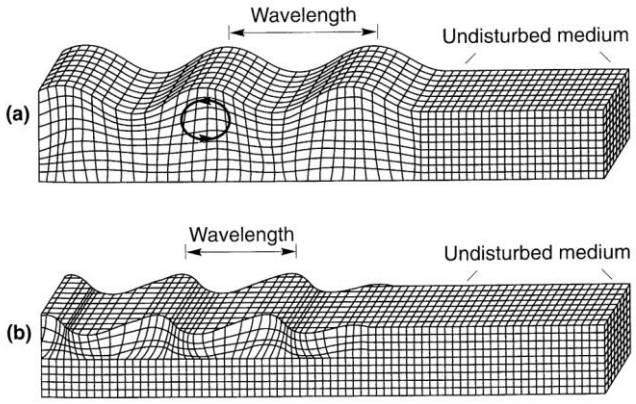

Figure 2.2. Surface wave motion propagation for (a) Rayleigh wave and (b) Love wave [6]

Rayleigh wave velocity is usually lower than S-wave velocity traversed through the same soil media. An in a elastic homogeneous media, R-wave becomes non-dispersive, meaning that the wave will be independent of the frequency. In that scenario, R-wave equation can be rewritten as [10]:

$$V_R = \frac{0.874 + 1.11v}{1 + v} \cdot V_s$$

Where v – Poisson ratio and V_R and V_s are Rayleigh wave and S-wave velocity

However, for a heterogenous and layered medium, surface waves reveal a dispersive behavior, which means that their velocity is directly related to the frequency of a generated wave. This, in turn allow us to generate surface waves, in particular Rayleigh waves, at different frequencies, and based on its propagation to the media conduct geophysical site test analyses (Figure 2.3)

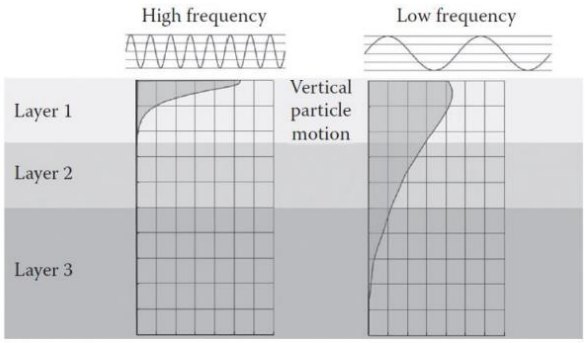

Figure 2.3. Dispersive nature of Rayleigh wave [8]

2.2. Geophysical site tests and methods

Commonly, borehole logging is utilized for the in situ geotechnical site investigation procedures and for extraction of soil samples for its further lab test analyzes [11, 12]. Even though such a procedure will provide a result of accuracy, it is necessary to repeat it several times to cover an area of interest. By doing so it is also necessary to find an optimum distance between tests, interpolation of which will provide adequate results and still will not require huge amount of borehole logging procedures. As an area of interest increases, the procedure might become expensive and time consuming. Even in a smaller survey areas geophysical site tests can be a better option, especially in a highly urbanized territories, where it is problematic to conduct noisy works or plant a special equipment for monitoring works. Moreover, due to its invasive nature, it is not considered as environmentally friendly way of extracting the stiffness information of soils as well [11, 13]. Geophysical surface wave tests in turn does not require a heavy special equipment and due to its portable nature easy to handle. Moreover, since in some of surface wave tests, there is no necessity to borehole log procedures, it becomes a quite cost efficient as well [13, 14].

The first attempts on using multi stations for surface wave techniques were in 1980s [15], but those attempts were limited by the computation speed of equipment, and it became more popular in 90s and 00s. [8] mentions that methods utilizing multichannel-array concept had highly raised the data processing quality in terms of reducing the subjectivity of the results and reducing the time for the final result.

Geophysical surface wave tests utilize the next two properties of surface waves: easiness of generating Rayleigh waves, and dispersive nature of surface waves. Thus, site tests are utilized as an alternative for traditional borehole logging and practiced for : identifying site's stiffness and geotechnical properties [12, 16-19].

Geophysical site tests itself are categorized as reference tests and non-reference tests. Former test utilizes an idea of comparison between the recordings being one of them as a reference data because of its location on or very close to the hard rock. The latter test comes in handy in cases where it is not possible to estimate the hard rock outcrops/bedrock signal data directly. Non-reference tests usually assumes that one of recorded data components contain original ground motion data, and that can be somehow extracted [20]. Active and passive Multichannel Analysis of Surface Waves (MASW) and Horizontal to Vertical spectral ratio (H/V) can be highlighted as a non-reference site tests. Those tests were used as an alternative for borehole log works [13, 18], for site response analysis [21], and site classification works [21, 22]. Standard Spectrum Ratio tests (SSR) can be classified as a reference test, which directly compares site amplification differences between soft soil and hard rock (outcrop).

2.2.1. MASW

Multichannel Analysis of Surface Waves (MASW) technique was first reported by [2]. It utilizes the dispersive behavior of surface waves via either generating Rayleigh waves from strong impact of sledgehammer into the metal plate, or by using the intact noise coming from an environment itself (e.g. traffic noise). Based on a nature of signal source, MASW technique can be divided into Active and Passive [23]. MASW technique itself was evolved from another surface wave test called Spectral Analysis of Surface Waves (SASW), from which MASW gained all the advantages of former technique and improved its drawbacks. Comparison of these two techniques can be seen from [10, 24]. In both, Active and Passive MASW, procedure consists of three main steps called 1) data acquisition, 2) data processing and 3) inversion of dispersion curve.

Active MASW method utilizes the dispersive high-frequency nature of Rayleigh waves generated by force, usually the strike of sledgehammer to the steel plate (Figure 2.5 & 2.4.a). High frequency waves will propagate to the shallow depth of the heterogeneous soil (Figure 2.3). For that reason, non-destructive Active MASW method is favorable for near-surface site characterization purposes. At the same time, due to the low frequency nature of ambient noises Passive MASW is better for estimating stiffness properties of higher depths of heterogeneous soil (Figure 2.3). Whole procedure for Active MASW procedure is illustrated below:

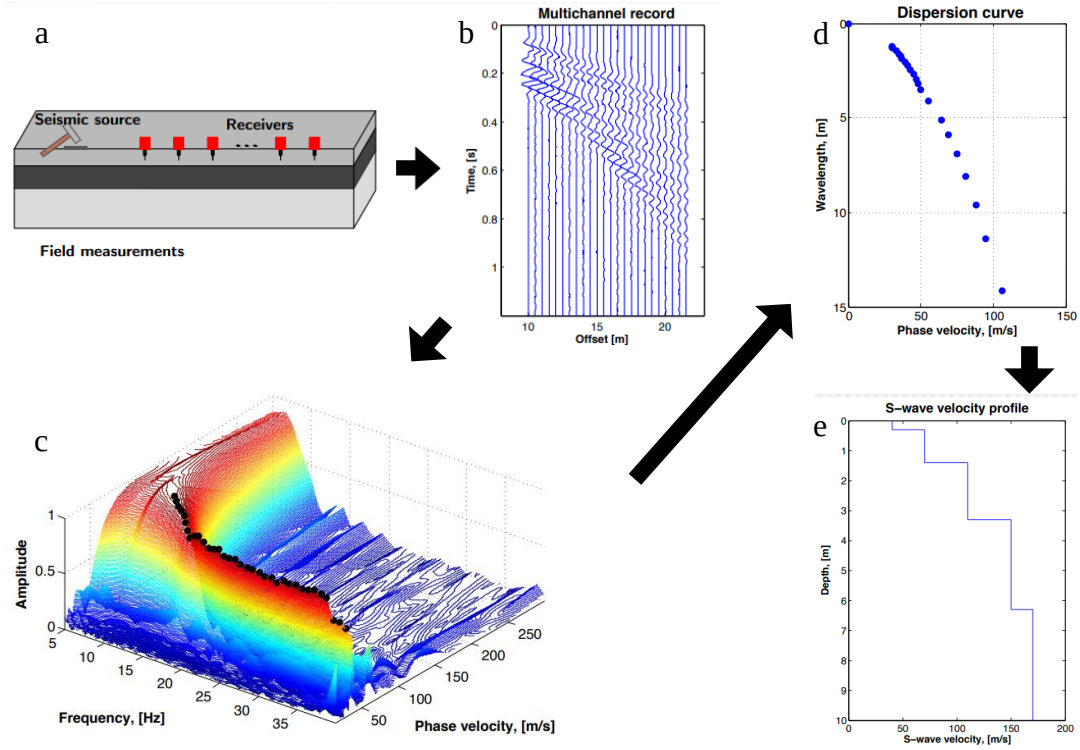

Figure 2.4. Active MASW. a) Field data acquisition; b) Result of data acquisition stage; c) Data processing result – Dispersion curve; d) Dispersion curve of fundamental mode; e) Inverted Vs profile [10].

2.2.1.1. Data acquisition

For Active MASW, data acquisition is done via linear array of uniformly spaced geophones (typically from 24 to 48, with a spacing of 0.5m to 2m). Geophones will record the ground shaking in response to the actively generated artificial vibration with a known source: usually by sledgehammer. Maximum survey depth that can be reached from this method depends on a several factors like receiver spread, source offset and geophone spacing [10], but usually it is said to be 30m. To avoid aliasing effect sledgehammer shots needs to be repeated several times.

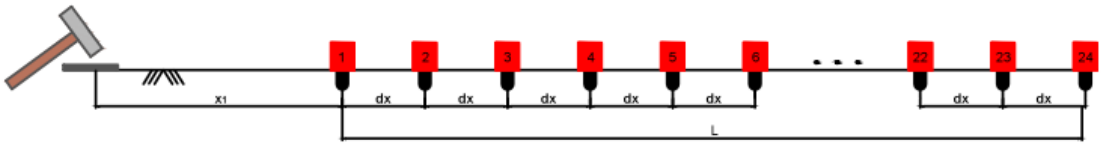

Figure 2.5. Field test configuration

For Passive MASW method, geophones will record the ground vibrations in response to the unintentionally generated ambient noises. Absence of information regarding the source of vibration and its distance makes it problematic to rely on linear geophones placing like in an Active MASW. Thus, geophones usually put in a regular shape geometry (Figure 2.6). However, such shapes are problematic and time consuming due to the complexity of the shape and possible presence of natural disturbances (like rocks or tress). Moreover, it is also problematic to follow a regular shape in an dense urban area. At the same time research as [12] have shown that a linear array at right angle with 11 geophones have lost insignificant details in comparison with regular shaped Passive MASW. Linear array is at the same time easier to implement in an urban area, especially close to the roads. Result of data acquisition stage in both cases will be the recordings of geophones in a time-space domain.

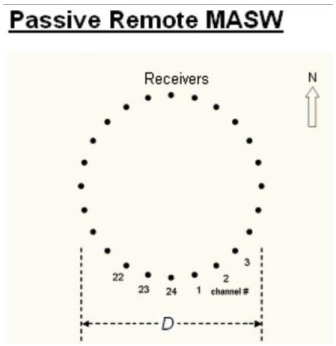

Figure 2.6. Passive array configuration example [23].

2.2.1.2.Data processing

The aim of data processing step remains the same for both Active and Passive cases: dispersion curve generation from available time-space domain recordings. Due to the dispersive nature of surface waves, it is required to analyze the recorded signals in a frequency domain. To do so, acquired signals are of time to space domain is transformed into frequency to either velocity or slowness or wavenumber. For Active MASW, there are several transformation ways of geophone recordings into the dispersion curve practiced in literature like like: slant-stack (Foti 2014,, McMechan 1981), frequency-wavenumber (FK) [25, 26]; swept frequency [10] and phase shift [13, 27]. For Passive MASW usually Spatial Autocorrelation (SPAC) method

is used. Geophone recordings might contain information of higher mode waves, but usually, inversion of fundamental mode of Rayleigh wave is of a primary interest [8].

2.2.1.3.Inversion

Inversion is last stage of MASW both methods which uses previously estimated dispersion curves for generation of stiffness profiles. This is an iterative process, that will find a best fitting Vs profile by comparing theoretical dispersion curve of the given profile with experimental dispersion curve estimated in data processing stage before. Iteration process is conducted by the next assumptions: soil layers are horizontal, no S-wave velocity change in one soil layer and each soil layer shows homogeneous and isotropic properties. The latter assumption helps to refer to the equation between Rayleigh wave and S-wave velocities, and by doing so helps to estimate S-wave velocities from surface waves. Inversion results are evaluated based on a misfit value of a model estimated by the next equation:

$$Misfit = \sqrt{\frac{1}{N}\sum_{i=1}^{N}\left(\frac{x_{r,i} - x_{c,i}}{\sigma_i^2}\right)}$$

Where $x_{r,i}$ and $x_{c,i}$ are reference phase velocity and inversion estimated phase velocity for a given frequency of f_i, N – number of inversion samples and σ_i – standard deviation.

Inversion process might result in a non-unique solution, meaning that the different Vs profiles will have the same misfit value. For that reason, final model should be visually double checked as well. Moreover, presence of extra geotechnical (e.g., knowing S-wave velocity of a certain soil layer) or geophysical (e.g., presence of another test results) or geological (e.g., soil and rock formation depth) information will help to mitigate the problem of non-uniqueness.

2.2.2. HVSR

Horizontal to Vertical Spectral Ratio (HVSR) method firstly described by Nogoshi and Igarashi in 1971 became more popular due to the works of [1]. Like a Passive MASW method, HVSR method utilizes a low frequency ambient noise of an environment. But it utilizes only one geophone capable of reading microtremors in three directions (2 horizontal and 1 vertical) for a long time period. HVSR method provide an information in terms of amplitude and frequency. The factor affecting an amplitude is reported to be a soft soil velocity (stiffness) and signal source itself. The mechanism of HVSR method is not fully explored, however, all works agree on fact that peak amplitude frequency corresponds to the natural frequency of soft soil. Microtremor wavefield contains mostly Rayleigh waves and Love waves [8]. In that case

microtremors in vertical direction might be considered as purely affected by Rayleigh waves, whilst horizontal direction microtremors will contain both Rayleigh and Love waves. Such contribution of surface waves into HVSR spectrum was explained by a surface wave motion direction: Rayleigh waves can make a ellipsoidal particle motion in both horizontal and vertical directions, whilst Love waves are traversed only in a horizontal direction [8, 28]. There are also attempts to eliminating Love wave effect into HVSR graph, thus conducting analysis on Rayleigh wave only. Such modification of HVSR graph is called Rayleigh wave ellipticity curve, or just ellipticity curve and will be described in a corresponding subsection.

For that reason, the method is commonly used for estimating the natural frequency of soft sediment layer using one of two equations, that are using arithmetic and geometric horizontal averaging approaches:

$$HVSR(f) = \frac{\sqrt{N^2(f) + E^2(f)}}{\sqrt{2} \cdot Z(f)}$$

$$HVSR(f) = \frac{\sqrt{N(f) \cdot E(f)}}{Z(f)}$$

Where, N(f), E(f) and Z(f) stands for spectral amplitude in north, east and vertical directions at a frequency f respectively.

[29] aimed to assess efficiency of different averaging techniques, however, in literature both averaging methods are practiced [3, 4, 30, 31]. It is also not been fully investigated whether if peak amplitude of HVSR graph corresponds to the local site amplification factor or not. Researches like [1] concludes that an amplitude is in trend with site amplification factor, whilst others [14, 31] claim that there is no strong correlation between those two factors. Moreover, researchers like [32] highlight that HVSR amplitude itself is not constant for a long period of time and must be carefully analyzed before making any conclusions.

As proposed in the SESAME project guidelines [33], there are 3 criteria for a reliable HVSR curve and 6 for reliable HVSR peak. Results satisfying those criteria might be used for estimating the depth of high impedance ratio which corresponds to the bedrock depth. To do so, three-component geophone recordings in time-space domain are split into components of a duration of usually less than a minute. Resulting recordings are visually assessed, and possible recordings affected by active vibrations or other higher noises are removed. For each remaining time windows results are transformed from time-space domain into frequency-amplitude

domain. Resulting signals are then smoothed with a Konno-Ohmachi filter. Konno-Ohmachi filtering in some cases allowed getting a spectral amplitude, which is equal to the site amplification factor. Such phenomena was especially appeared for a sites where Rayleigh waves were of 0.4 of all contained microtremors of the site [34]. Figure 2.7 demonstrates a) division of three-component signal recordings into time-windows, followed by b) estimation of average HVSR along with HVSR for each time-windows. Color spectra in each HVSR corresponds to the time-windows in Figure 2.7a.

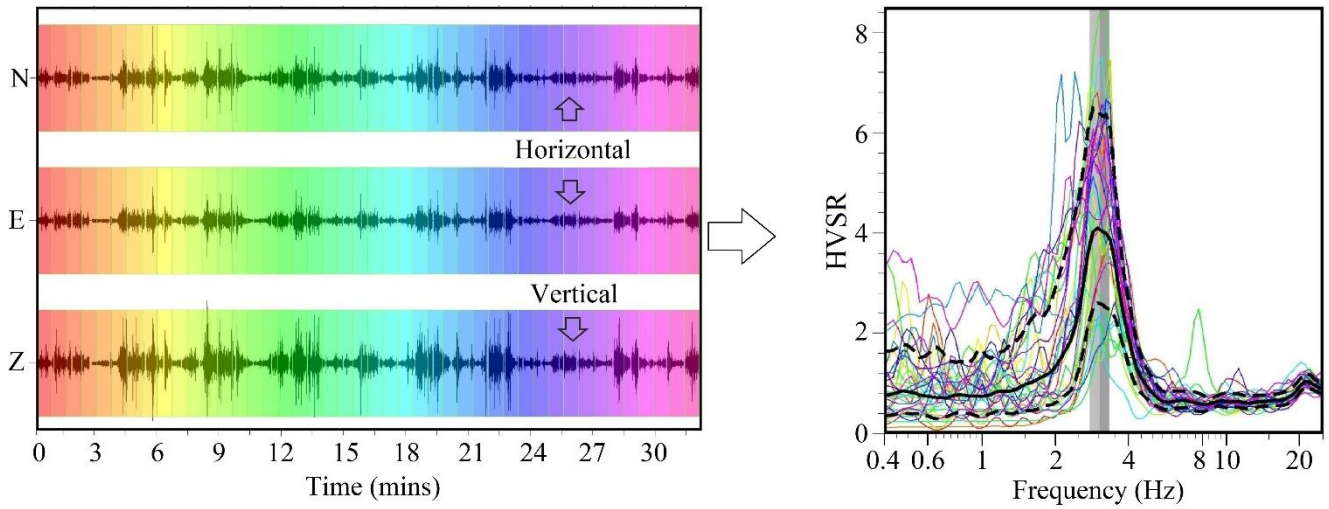

Figure 2.7. HVSR test results(a) selected time windows in three component geophone recordings, (b) HVSR graph for each of time windows

Natural frequency of the soil also indicates sharp impedance contrast depth, where in heterogeneous isotropic soil media soft soil layer is shifted by hard rock layer (bedrock) [29, 35, 36]. Impedance ratio itself is estimated following the next equation:

$$IC = \rho_2 V_{s,2} / \rho_1 V_{s,1}$$

Where ρ2 and ρ1 are densities of lower and upper layers, and Vs2 and Vs1 are S-wave velocities of lower and upper layers of soil. At a hard rock both density and S-wave velocity will rise drastically, revealing an increase of IR at the depth of bedrock.

HVSR curves that satisfy all the requirements of SESAME project can be used for estimating the bedrock depth of the soil layer. This is because of high impedance contrast that corresponds to the peak amplitude and corresponding frequency of HVSR. Quarter wavefield equation is utilized for an estimation of a bedrock depth:

$$H = V_{s,aver} / 4f$$

Where H corresponds to the depth from surface to the strong impedance ratio, f is natural frequency of the soil, and Vs is the average S-wave velocity above strong impedance ration. $V_{s,aver}$ in its turn can be measured following the NEHRP recommendations as follows [37]:

$$V_{s,aver} = \frac{\sum_{i=1}^{n} H_i}{\sum_{i=1}^{n} (H_i / Vs_i)}$$

Moreover, along with quarter-wavelength method shown above, bedrock depth can be estimated using exponential reduction equation:

$$H(f) = a \cdot f^{-b}$$

Where, a and b are site specific parameters. There are several site-specific reduction parameters, like [38-40],which allows to determine bedrock depth from a natural frequency of the soil layer.

2.2.2.1.Earthquake HVSR

Earthquake HVSR is also a single-station method that is not rely on a reference signal recording. It shares the same principle as an ambient noise HVSR method, however, utilizes an earthquake signal propagation through earth crust, especially S-wave component, for an estimation of HV spectral ratio. The method follows an assumption that vertical ground motion will not be affected by site and ground amplification effects and represents original signal at the bedrock level. Shear wave method was assessed in terms of natural frequency of soft soil layer [41], and correlation between site amplification and amplitude of earthquake HVSR results. Even though it was said that conventional HVSR amplitude is biased and might not be linked to the site amplification, it is revealed that Earthquake HVSR amplitude might be utilized as a lower bound for site amplification factor [41].

2.1.1.1.Possible challenges with the HVSR measurement

Due to the easiness that HVSR test provides, it became very popular in a seismology and in geotechnical engineering as well. With a rapid growing of the test, there was an urge in standardization procedures of the test itself. SESAME project (2004) aimed in evaluating possible scenarios affecting to, and standardization of guidelines for the data acquisition, its processing, and its final result as well. As a result, effects of different parameters were evaluated and recommendations are suggested. It is reported that for low frequency spectra, common problem that can be faced during stable HVSR curve acquiring is weather effects, and artificial noises (e.g., factories, cars, etc). Moreover, parameters like recording duration, location, its

spacing and presence of nearby structures (e.g., factories, pipelines) will also affect to the final result and must be assessed properly. All mentioned parameters will affect to the final HVSR curve and their role must be taken into consideration, however, it was also suggested a criteria for reliable HVSR curve and clear HVSR peak as well. However, since field survey conditions, and especially geotechnical properties of the soil cannot be controlled and in most of the time cannot be known before the test conduction.

2.2.3. Ellipticity curves

H/V profile spectrum contains surface wave contribution effect from Rayleigh wave and Love waves. However, minimization of effect of Love waves will help to utilize H/V information for S-wave profile inversion like seismic site surface tests (e.g., MASW). There is a mismatch between the results of HVSR curve and Rayleigh wave's ellipticity curve [42]. Due to the absence of Love waves in ellipticity curve's horizontal noise wavefield component, for all frequencies ellipticity curve will show lower spectral amplitude than HVSR [42]. However, close to the natural frequency, ellipticity curve will tend to infinity. Researchers like [43, 44] had explored an effect of natural frequency amplitude in ellipticity curves and concluded that close to the natural frequency, soil layer lose its ability to conduct seismic vertical noises. Presence of remaining wave contributions at natural frequency can be linked to the refraction and reflection of seismic waves.

2.2.4. Ellipticity curve extraction

There are at least four methods for ellipticity curve extraction from geophysical tests. Two of them using single three component time-space ambient noise recordings, and the remaining two using array methods [45]. Here single component ellipticity curve inversion techniques (RayDec, HVTFA) will be described. First method is RayDec method [46] and the latter is Time-frequency analysis via Continuous Wavelet Transform method introduced by [47]. Both methods are based on a phenomenon of quarter period phase delay between horizontal and vertical components of surface waves, whilst for body waves there will be no delay in motion. The latter method is utilized in a Geopsy software [48, 49] and had been conducted in this study.

RayDec method

For RayDec method, for each frequency value the next operations are repeated, and based on that ellipticity to frequency curve will be plotted. All three components are firstly filtered out using Chebyshev filter with a central frequency of f and a bandwidth of df. Further

sensitivity analysis of study have shown that an optimum filtering bandwidth was *df*=0.2f. To focus on an Rayleigh wave contribution to the filtered signals vertical component is assessed for a sign change in time-amplitude space. For all cases, where sign change presents (τ_i), time windows with an optimum length of $\Delta=10/f$ are stored with respect to quarter period delay ($0.25f^{-1}$) between horizontal and vertical components:

$$v_{b,i}(t) = v(\tau_i + t)$$

$$e_{b,i}(t) = e(\tau_i + t - 0.25f^{-1})$$

$$n_{b,i}(t) = n(\tau_i + t - 0.25f^{-1})$$

Where, i stands for an order of appearance of sign change cases in a vertical signal after applying Chebyshev filter; *v,e,n* are vertical, east and north signal components, respectively.

Unlike a common HVSR horizontal component averaging technique described in section 2.2.2., RayDec processes an estimation of maximum correlation angle between north and east signal components. A maximum correlation angle might be different for each group of three component signals, and will be estimated via the next correlation equation:

$$\theta_i = \tan^{-1}\left(\frac{\int_0^{\Delta} v_{b,i}(t) \cdot e_{b,i}(t)dt}{\int_0^{\Delta} v_{b,i}(t) \cdot n_{b,i}(t)dt}\right)$$

Each horizontal component is then will be equal to the sum of the sine projection of east component and cosine projection of north component. For a selected time-windows and corresponding horizontal and vertical signals, Body waves and Love wave will affect apparently. For that reason, for each selected time windows correlation between horizontal and vertical will be assessed. Depending on the nature of the signals, correlation might be high when Rayleigh wave dominates or vice versa. Thus, the next correlation equation will be applied:

$$c_i = \frac{\int_0^{\Delta} v_{b,i}(t) \cdot h_{b,i}(t)dt}{\sqrt{\int_0^{\Delta} v_{b,i}^2(t)dt \cdot \int_0^{\Delta} h^2(t)dt}}$$

After that, all time windows are stacked up by emphasizing their correlations, and ellipticity for a selected frequency value will be estimated from an energy ratio of horizontal and vertical stacked signal components:

$$v_S(t) = \sum c_i^2 \cdot v_{b,i}(t)$$

$$h_S(t) = \sum c_i^2 \cdot h_{b,i}(t)$$

$$\epsilon = \sqrt{\frac{\int_0^{\Delta}(h_s(t))^2 dt}{\int_0^{\Delta}(v_s(t))^2 dt}}$$

The method assess the correlation between horizontal and vertical signals, which helps to enhance the contribution of Rayleigh wave component in wavefield. For a long signal durations (depending on an expected fundamental frequency, it will be 5min or higher), stacking of all such time-windows with respect to the correlation weight of horizontal and vertical components will result in an ellipticity value for a given frequency. Repeating the procedure for all frequencies, will end up by plotting Ellipticity curve.

Time-frequency method

Time-frequency method, also known as Horizontal to Vertical Time-Frequency Analysis (HVTFA) is another method for estimating ellipticity curve. Technique adjusts wave energy arrivals and utilizes continuous wavelet transform (CWT) of three signal functions with wavelet function separately:

$$CWT_{x(t)}(a,b) = \frac{1}{\sqrt{|a|}} \int_{-\infty}^{\infty} x(t)\, \psi^*\left(\frac{t-b}{a}\right) dt;$$

Where $\psi^*\left(\frac{t-b}{a}\right)$ is a scaled and translated wavelet function ($\psi(t)$) via parameters "a" and "b", $x(t)$ is noise recordings of three component signals. For HVTFA modified Morelet function is used as a wavelet [49]:

$$\psi(t) = e^{j2\pi v_0 t} \cdot e^{-t^2/N}$$

Result of CWT will be three-dimensional time-frequency graph, where each signal component's amplitude described as its frequency composition, and its position in time. TF representations of two horizontal signals then merged via vector sum and TF representation of vertical signal would be considered as reference data in further estimations of Rayleigh wave contribution [49-51]. TF representation demonstrate multiresolution property: they will have high resolution in frequency/low resolution in time for low frequency ranges and vice versa [49, 50]. To improve the reliability of results, time axis is usually split into time windows of one minute [51]. For HVTFA, ellipticity at a certain frequency is estimated as a ratio between vertical maximum and the horizontal amplitude. Horizontal amplitudes for each frequency are phase-shifted in ($1/4f_{i,n}$) in comparison with vertical maxima time ($t_{i,n}$). As a result, ellipticity

curve is estimated as a ratio of horizontal amplitude to the vertical maxima and plotted in log scale. The same procedure is repeated for each frequency and time window.

2.2.5. Ellipticity curve inversion

Similar to the dispersion curve inversion in MASW, Ellipticity curve inversion procedure will conduct a back problem solving via generating Ellipticity curves for a soil property indicated in parameter space for inversion (Vs, Vp, density, Poisson's ratio). For the Geopsy software, inversion procedure is organized by Neighborhood algorithm, that for each group of parameter space input will estimate a Misfit value and based on its value will or won't assess parameter space close to the assessed value. Such evaluation of parameter space zones will help in better solution searching results [52, 53]. During an inversion procedure, each model's credibility is assessed via Misfit criteria shown below, and the model with the lowest misfit is believed to be the solution of inversion procedure.

$$Misfit = \sqrt{\frac{1}{N}\sum_{i=1}^{N}\left(\frac{x_{r,i} - x_{c,i}}{\sigma_i^2}\right)}$$

Where $x_{r,i}$ and $x_{c,i}$ are reference and calculated ellipticity amplitudes for the frequency value f_i, σ_i stands for standard deviation between the results, N is number of samples.

Like the Rayleigh wave phase velocity inversion (dispersion curve), Rayleigh wave's ellipticity curve inversion might result in a non-unique Vs profile(e.g., [4, 50, 54]). In case of three component signals, this issue is even more problematic than in dispersion curve, because it was shown that scaling Vs profiles will not affect into the ellipticity curve. Moreover, Neighborhood algorithm is classified as a global search algorithm, and in case of misidentification of parameter space, there is a possibility to that algorithm might take huge time for inversion and still won't converge [54]. A-priory known geotechnical or geophysical information in site will help to prevent non-uniqueness issues for inversion [11]. Especially, fixing or minimizing possible values for Vs of the uppermost soil layer will help for preventing model scaling.

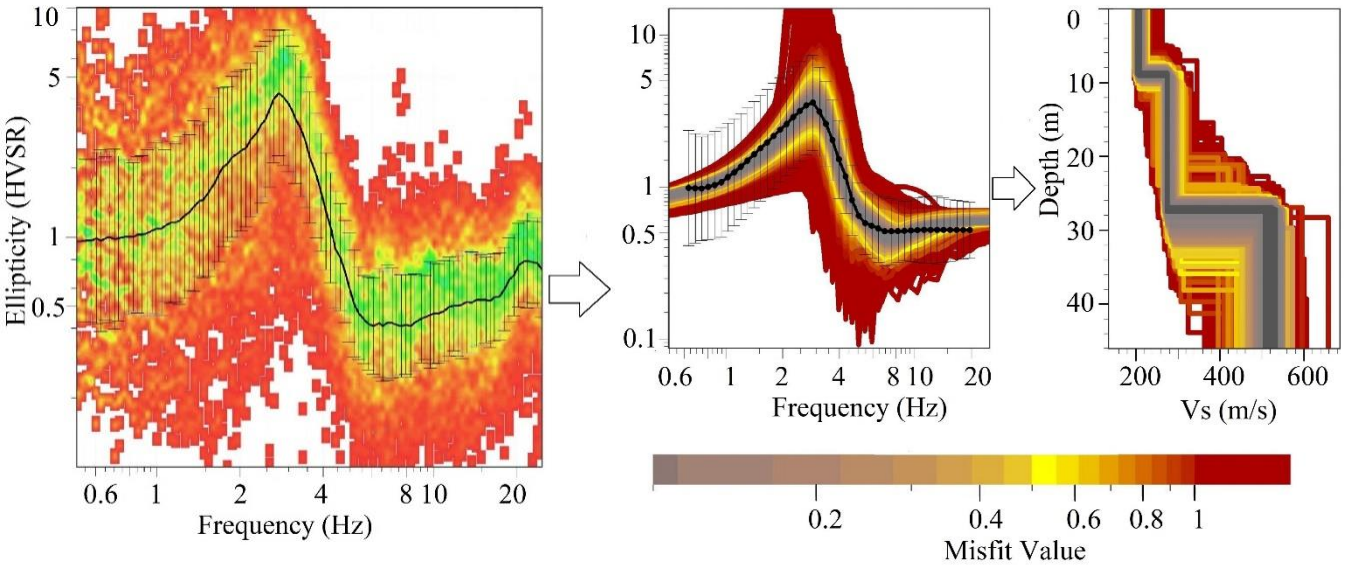

Figure 2.8. Ellipticity inversion process at the test site (S2): (a) Ellipticity curve obtained from CWT, (b) Modelling ellipticity curves, (c) Vs profile modelling

Figure 2.8 illustrates (a) ellipticity curve generated via HVTFA method, and its further inversion procedure: comparing ellipticity curves between HVTFA and artificially generated models (b) and their Vs profiles. Red to green spectral distribution in Figure 2.8 (a) stands for a energy distribution dynamics where green stands for high and red for low; whereas red to grey spectral distribution in Figure 2.8 (b) and (c) stands for model's misfit.

2.2.6. Standard spectral ratio

The SSR technique is also a reference site method [20]. In fact, once a reference site has been chosen, the spectral ratios between all the other stations and the reference are calculated for each component of ground motion. Reference based site test utilizes a principle of the same sources and effects on propagation are considered in records from the reference site (station at outcrop) as in records from other sites [55-57]. This method is applicable when the distance between evaluating stations are much lower in comparison with their epicentral distance, which may imply that stations are recording the same signal, but at different site conditions. This ratio can be calculated independently for each of the three components, namely vertical (Z), north–south (N), and east–west (E), however it is commonly used to average horizontal spectra [58]. As a result, the SSR can provide the results of site response [59].

2.3. Seismic Site classification

Seismic site classification procedures are conducted in accordance with the recommendations of the National Earthquake Reduction and Prevention (NEHRP) program and based on an estimation of average S-wave velocity of the site. In particular, based on

average S-wave velocity of an upper 30m of site. In case of there is no possibility to measure it directly, empirical correlation equations among other in-situ tests are allowed (e.g., N count from SPT, tip resistance from CPT, etc.). In case of utilizing empirical correlation equations, possible uncertainty in results must be considered by estimating site classification for S-wave velocity profile interval with plus and minus 30% boundary for empirically derived S-wave velocity. In case when interval will reveal different site classes, the most critical site class for each period must be selected via engineer. Calculated S-wave velocity must be distance averaged using the next equation:

$$V_{s,avg} = \frac{\sum h_i}{\sum h_i / V_{s,i}}$$

Where, h_i and $V_{s,i}$ I corresponds to the depth and S-wave velocity of i-th soil layer. Commonly average S-wave velocity of 30m is used for site classification procedures ($\sum h_i = 30m$) and are based on a Table 2.1 below:

Table 2.1. Site classification criteria [37]

Site class		$V_{s,30}$
A.	Hard rock	more than 1500 m/s
B.	Firm to hard rock	760 – 1500 m/s
C.	Dense soil and soft rock	380 – 760 m/s
D.	Stiff soil	180 – 360 m/s
E.	Soft soil	less than 180 m/s
F.	Special cases	

2.4. Numerical modeling

Numerical modelling techniques are used for assessing site's response under dynamic loads and static load effect. Among the geotechnical problems solved via numerical modelling, dynamic analysis is conducted to research on possible reasons of occurred landslide and slope stability failure, or to study and assess landslides caused by flooding. It is also utilized for an assessment of site amplification issues during the dynamic input signals. Numerical modelling demands a geotechnical and geophysical information of site, that is commonly taken from lithological, geological and sediment site maps, as well as from the borehole logs and site investigation tests. In most of researches like ([60-62]) 3D Geomodel is first generated, with further analysis of 2D or 1D sections in using DEM software (e.g., UDEC, 3DEC, Flak3D) [63, 64]. For this work, 3D Geomodel is generated using borehole logs, geology and sediment layer

maps using LeapFrog software, with further analysis of 2D sections for dynamic response in UDEC.

2.5. Seismic Site microzonation

Seismic site microzonation is one of key procedures linking earthquake engineering with structural engineering; procedure is aimed to assess potential earthquake damage for its further mitigation. Seismic microzonation in general tends to assess the earthquake hazard safety for structures affected by dynamic loading (earthquake) and for site itself against earthquake generated scenarios like site amplification, liquefication, slope instability due to the dynamic loadings [65, 66]. Seismic site microzonation in turn might be focused on a particular phenomenon causing earthquake hazard, such as ground motion or liquefaction potential or slope instability failure potential assessment. Based on degree of potential local site hazards, zonation map resolution might be different as well: starting from general scale maps to detailed and rigorous maps. Resulting maps are demonstrated in a spreading of dynamic soil properties over an analyzed area. It was previously demonstrated that S-wave velocity ratio between soft soil and bedrock layers are highly correlated with site amplification factor. Thus, microtremor data can be used for generation of detailed maps with a scale of 1:100 000 to 10 000 [65]. Along with average S-wave velocity seismic microzonation is presented in terms of natural soil frequency values and HVSR peak ampltudes [51, 62] (despite not being fully correlated with site amplification factor).

Chapter 3. Seismic site classification of Singapore: case study

3.1. Introduction

Increase in urbanization level of the region results in a constant demand of site investigations for 1) structural engineering and evaluation of sustainability of constructions to the dynamic loads like earthquakes, 2) detailed investigations of soils for better foundation designs with a minimization of resources and prevention of site effect phenomena like liquefaction, slope instability and site amplification, but for sufficient factor of safety recommended by local building codes. For reaching such requirements investigation of soil's dynamic soil properties are demanded. This chapter in an example of Singapore data, focuses on an implication of HVSR technique data for site classification and further potential of seismic microzonation. It is believed that HVSR data to be quite a handy for achieving the task of investigating crowded areas, especially because of its portability, low scale of overall equipment size followed by key working mechanism: it requires an ambient noise.

3.2. Site Locations and data

Case study was conducted using three component signal and MASW recordings recorded previously as a scope of HVSR methods and used for evaluation of bedrock depth via MASW [18, 67] and HVSR tests [38]. As part of those works HVSR data was utilized for an estimation of fundamental frequency of site, for generation of bedrock depth to natural frequency correlation estimation works. This case study expands it more via presenting a method of ellipticity curve inversion of three component signal data of seven sites (S1-S7) and by comparing the results with MASW, which are considered as a reference. All seven sites are in a zone of Singapore island, where Bukit Timah Granite is the bedrock layer (figure 3.1a) and spreading of all seven zones can be seen from the figure 3.1b. The data spreading is non-homogeneous, meaning that results extrapolation for planed mapping zone (red square) will be highly biased. This issue was not taken into account at the beginning of the research works, leading to the misbelief in possibility of mapping natural frequency and HVSR amplitude map generation. Three seismic stations situated in Singapore are shown in figure 3.1a as well.

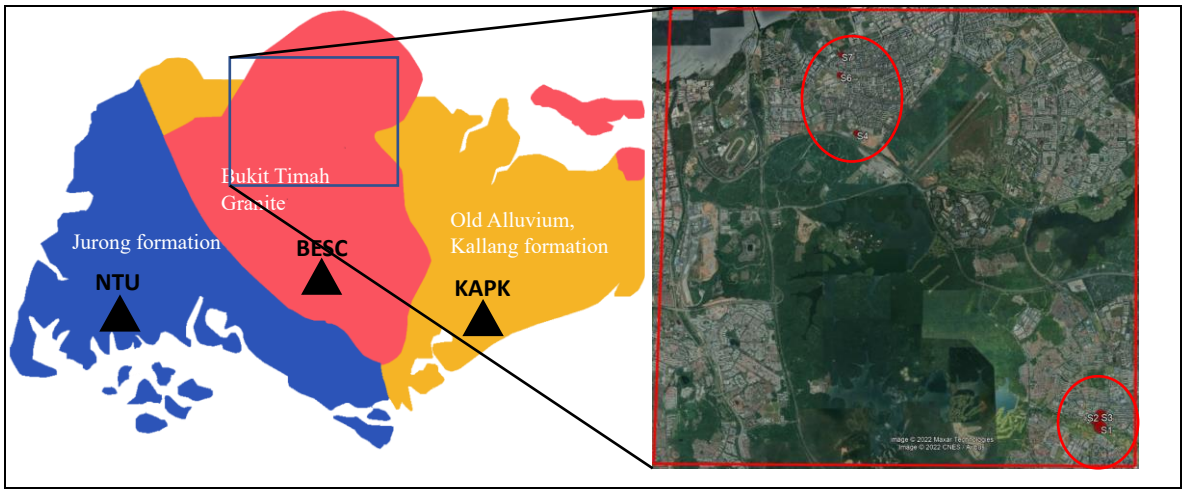

Figure 3.1. Singapore geology with 3 seismic stations and location of 7 three-component signal measurements (red circles) and numerical modelling border in Bukit Timah Granite.

Bukit Timah Granite territory consist of mostly granite and sometimes from diorite or adamellite rocks as a hard rock layer. Granite layer formed due to the hardening of magma formations. Key aspect of Bukit Timah Granite is presence of transitional weathered granite layer between hard rock and soft soil layer. Weathering depth changes is in average equals to 25m. For numerical modeling Bukit Timah Granite of weathering degree III or below is classified as bedrock layer due to the huge contrast in structural properties between III and II (Table 3.1).

Table 3.1. Bukit Timah Granite weathering degree classification [68]

Grade	Basis for assessment
I	Unweathered, hard rock. Hardly broken by hammer. Discoloration signs are not noticed.
II	Hardly broken by hammer. Rocks retain its fresh colors with staining near the joints.
III	Can be easily broken by hammer, but not by hand. Generates a dull so striking by hammer. Staining signs can be observed everywhere.
IV	Discolored rock. Can be easily broken by hand. Does not dissolve in water
V	Fully discolored rock. Can be easily broken by hand. Dissolvable
VI	No signs of rock structure. Dissolvable. Easily falls into pieces by hand

3.3. Methods

For all 7 three component signals, common HVSR and ellipticity curve inversion procedures were conducted via Geopsy software, with embedded HV and HVFTA functions. Ellipticity curve further inverted utilizing Dinver software. For HVSR method, processes

described in section 2.2.2 were conducted for a frequency range of 0.4 to 25 Hz due to the three component geophone specifications, with a time intervals of 20 to 25 seconds following SESAME clear peak and reliable curve criteria. Ellipticity curves were generated and inverted using software and following the procedure described in section 2.2.4.2 and 2.2.5 respectively. During an inversion procedure, parameter space for uppermost soil layer was defined with a reduced S-wave velocity interval (table 3.2) with an agreement of common soil type found in borehole logs (sandy silt, sandy clay and clayey sand). From Vs profiles generated from an ellipticity curve inversion procedure, Vs_{30} values were estimated and then used for seismic site classification procedures described in section 2.3. Results were compared with MASW based site classes and described in results section.

Table 3.2. Intervals for inversion model parameter space

Layer	Thickness (m)	Vp (m/s) min–max	Vs (m/s) min–max	Density (kg/m^3) min–max
1st	0–10	320–450	180–260	1700–1900
2nd	5–15	400–650	220–380	1800–2000
3rd	10–30	450–800	250–450	2000–2100
4th	25–50	600–1400	300–650	2200–2400

Chapter 4. 2D and 3D soil profile modeling in Singapore territory

4.1. Introduction

Singapore territory despite not being directly located in drastic active faults still affected by so called “fire ring” group of faults near Philippines, Indonesia. Ground shaking effect due to the close subduction zones is still can be felt in the city. Earthquakes of magnitude of 4.6mb or lower still can be observed by seismic stations of Singapore (table 4.1).

Table 4.1. Earthquakes occurred in Indonesia

Year	M.	D.	Time	Lat	Lon	Mag
2015	8	1	21:31:13	-0.31	101.27	3.6
2015	3	13	9:13:41	0.24	101.34	3.6
2014	9	27	12:44:49	-0.38	101.42	3.5
2013	8	10	19:54:42	0.18	101.77	3.6
2013	6	23	14:43:12	1.85	101.40	3.4
2012	5	22	1:03:53	0.76	100.92	3.2
2012	4	24	11:49:48	0.38	102.06	3.5
2012	4	10	23:12:22	1.09	101.63	3.5
2012	3	31	3:58:19	0.97	101.55	4.6
2012	3	29	13:43:31	1.12	101.56	3.9
2012	3	29	10:30:32	1.01	101.51	4.4

Earthquake engineering must be considered during the design of constructions and for assessing site effects like site amplification and liquefaction. Microzonation is commonly practiced method of mapping a different ground’s dynamic properties in earthquake hazard estimation. In this chapter, 3D Geomodel for Bukit Timah territory will be generated with a further 2D profile assessment with synthetic and real earthquake data.

4.2. 3D Geomodel

More than 200 borehole logs were inputted to generate soft sediment and weathered granite layers followed by satellite images utilized for elevation level of soft sediment layer. 3D Geomodel was simplified to have three soil layers: hard rock (Bukit Timah Granite), weathered transition zone and soft sediment layer. It became clear that available borehole log information is highly concentrated in center and central north (Figure 4.1.a), meaning that there might be high uncertainties in farthest zones of the model. Moreover, SESAME project [33]

suggest lower distribution distance between test results as well (500m or lower). Additional data in the form of synthetic boreholes summarized from geological maps were added (Figure 4.2.a). British geological survey ([69]) sediment formation maps and topographic maps correlated with depth of soft soil layer were utilized. Interpretation of input data with an interpolation and extrapolation along the whole modelling zone was conducted using the LeapFrog software.

Figure 4.1. 3D Geomodel input data a) borehole logs, b) borehole logs with synthetic borehole data

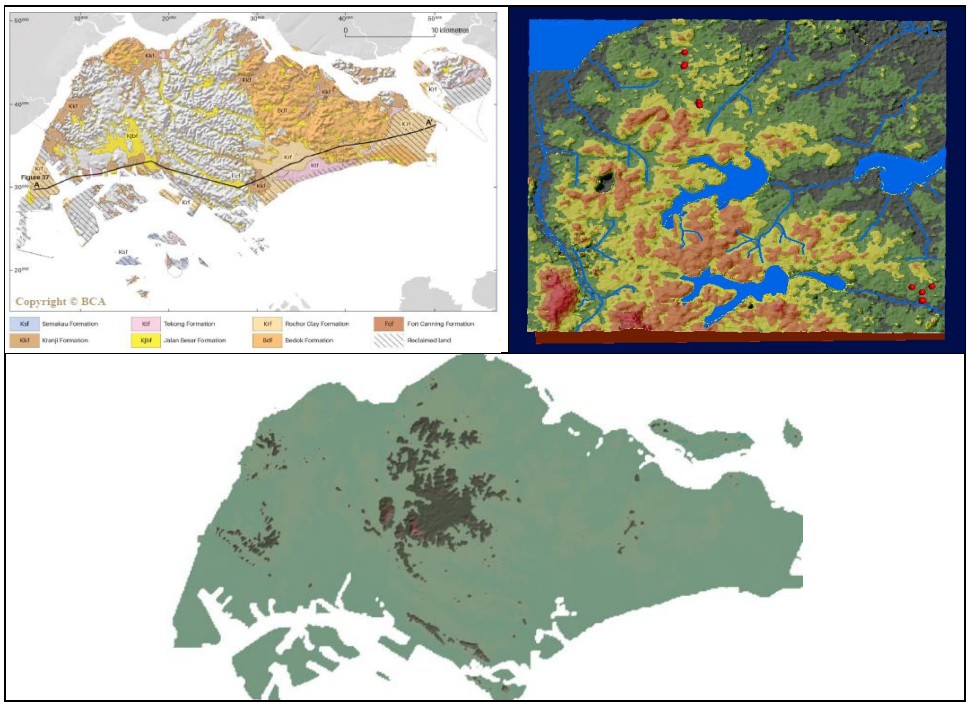

Figure 4.2. 3D Geomodel generation input data. a) location of all initially inputted borehole data, b) additional synthetic boreholes, c) sediment map, d) topography to soft soil depth correlation map, e) Digital Elevation Model

4.3. Methods

Resulted 3D Geomodel as shown in figure 4.2.a, by considering the locations of geophysical tests, was used for generation of 2D soil profiles figure 4.2.b. Further dynamic

analysis (acceleration-time history response of simulated geophones) of 2D profiles were conducted in UDEC software using Ricker wavelet signal, double signal and earthquake noises as an input signal generated at the bottom of the model (500m below the sea level). Simulated amplitude-time-history results were then utilized for a further analysis of HVSR of site using signal analysis software like Geopsy and following the procedure described in 2.2.2., for model's further validation. Input parameters for soil layers were taken as:

Table 4.2. Geotechnical properties of soft soil, weathered granite and hard rock

	ρ (kg/m3)	K (GPa)	G (GPa)	C (kPa)	θ (°)
Soft soil	1900	1.39	0.380	6	24
Weathered granite	2200	10.2	4.7	3	38
Bedrock	2600	14.2	7.7	Inf	

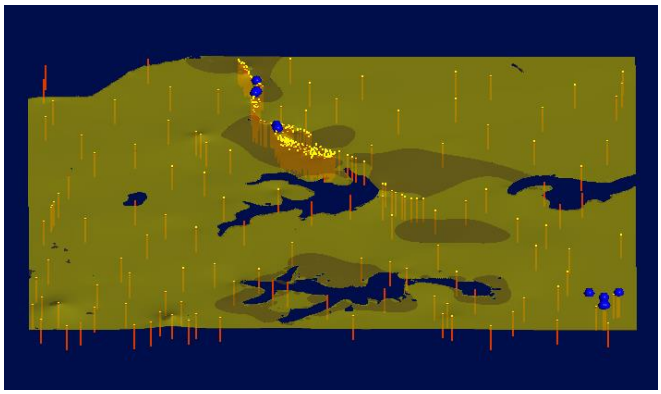

Figure 4.3. Top-layer of 3D Geomodel (transparent yellow) with input data: boreholes and geophysical tests (blue bubbles)

Ang Mo Kio Park

Marymond Rd.

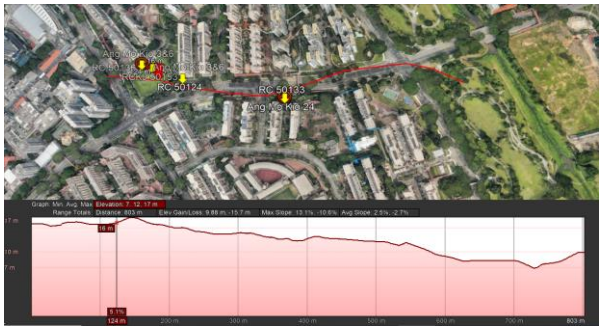

Figure 4.4. Example of 2D Soil profiles with borehole logs (yellow arrow) and geophysical test data (red circle)

Chapter 5. Results

5.1. HVSR

Noise HVSR for 7 sites were estimated using Geopsy software and shown in figure below. As it is recommended, Konno-Ohmachi filters were utilized for signals with a smoothing constant of 40. For each site time-windows' average HVSR results are generated, and clear peak and reliable curve criteria suggested via SESAME project [33] are applied. Resulting peak amplitudes and soft sediment natural frequencies are shown in table 5.1. Standard deviation in amplitudes and peak frequencies are automatically estimated via software demonstrated as a dashed lines (amplitude stdv), and light and dark grey bars (frequency stdv). Even though peak amplitudes cannot be directly linked to the site amplification coefficient, it is still a valuable and quick reference factor that can be used as a lower boundary of site amplification factor. For that reason it can be stated that f_0 and A_0 are crucial parameters for microzonation studies. Due to the geophone limitations and SESAME project recommendations, noise frequency was assessed in the range from 0.4 to 25 Hz. Resulting HVSR peaks correspond to the frequency interval of 1.9-3.4 Hz (Figure 5.1). According to the previous research results, derived from Active and Passive MASW [13, 18], for the Bukit Timah Granite zone, top sediment and hard rock S-wave velocities are in interval of 200–250 m/s for topsoil layer and 450–650 m/s for hard rock layer, such a variety in S-wave velocities along with the fact that hard rock density might not be lower that sot soil sediment, will result in a high impedance contrast in sediment. Thus, bedrock depth can be estimated using correlation between bedrock depth and quarter frequency [70]. Resulting bedrock depths ranges from 20.6 to 33.2 m, where the shallowest bedrock is believed to be in S2 and biggest depth in S5.

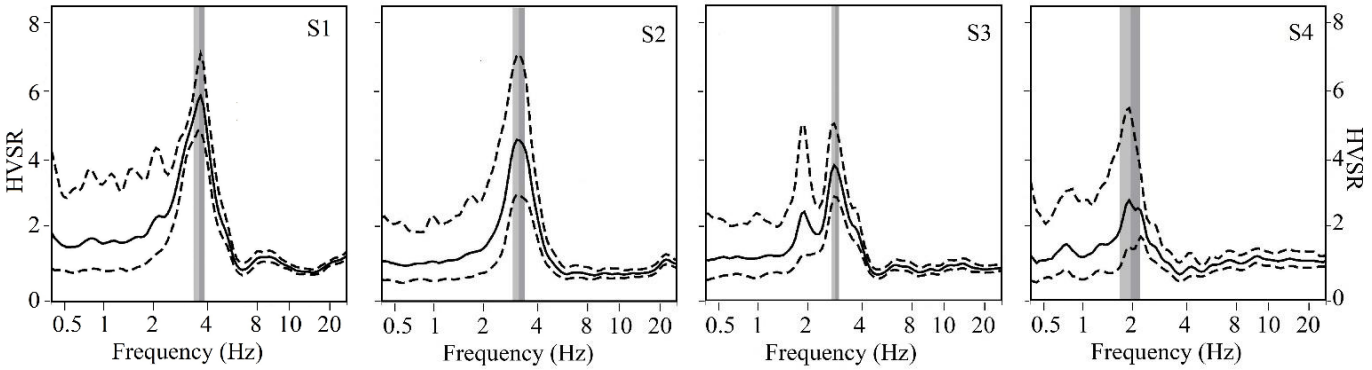

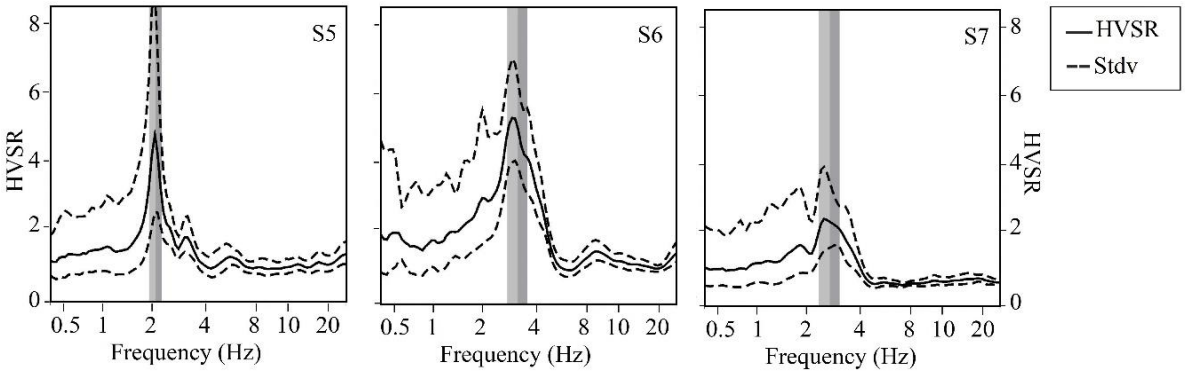

Figure 5.1. HVSR results in seven test sites

Table 5.1. List of investigated sites using the HVSR method in the territory of Bukit Timah Granite in Singapore

Site ID	f_0 (Hz)	stdv(f_0)
S1	3.4	0.22
S2	3.0	0.24
S3	2.7	0.14
S4	1.9	0.34
S5	1.9	0.25
S6	3.0	0.43
S7	2.5	0.43

5.2. Vs profiles from Ellipticity curve inversion

Vs profiles were estimated from the same three component raw signals utilizing ellipticity curve inversion procedure. Parameter space intervals for values like Vs, Vp, density and Poisson's ratio were provided based on a previous researches in Singapore territory [17], and borehole data. A-priori knowing the presence of very soft soil layer on top helped to reduce velocity interval in uppermost layer (shallow parameter space of 180-260 m/s) and prevent non-uniqueness of inversion process. Other layers' Vs intervals were set by slowly raising values due to the presence of stiffer soils at the bottom and due to the outcrop effect. Poisson's ratio is set to be in the range of 0.2 to 0.5: top layers 0.5-0.3 and bottom with 0.4-0.2. Based on the borehole log composition and depth of each soil formation, the Vs profiles are divided into three to four layers in the ellipticity curve inversion.

During the inversion procedure Ellipticity of Rayleigh wave's fundamental mode was estimated for each generated model in accordance with parameter space boundaries, and misfit between modeled ellipticity curve and HVTFA ellipticity curve is estimated. The result of inversion process will be best fit model with the lowest misfit value (red line in Fig. 5.2).

Fig 5.2 reveals resulting Vs profiles generated from inversion process along with MASW test results [13] that will be further utilized as a reference model in assessing site classification procedure.

5.3. Site classification

Presence of soft sediment soil layer will have a linear effect to the site amplification via the ratio in shear waves of bedrock layer to soft sediment layer. It has been noted that site effect has a destructive role in seismic hazard evaluation for site and local constructions [71-74]. Urge in site classification for further corresponding earthquake engineering presents for all earthquake affected zones. Seismic site classification procedure is of a technique utilized for an evaluation for its further consideration and construction design. National Earthquake Hazards Reduction Program (NEHRP) [37] suggests an application of average Vs of uppermost 30 m of

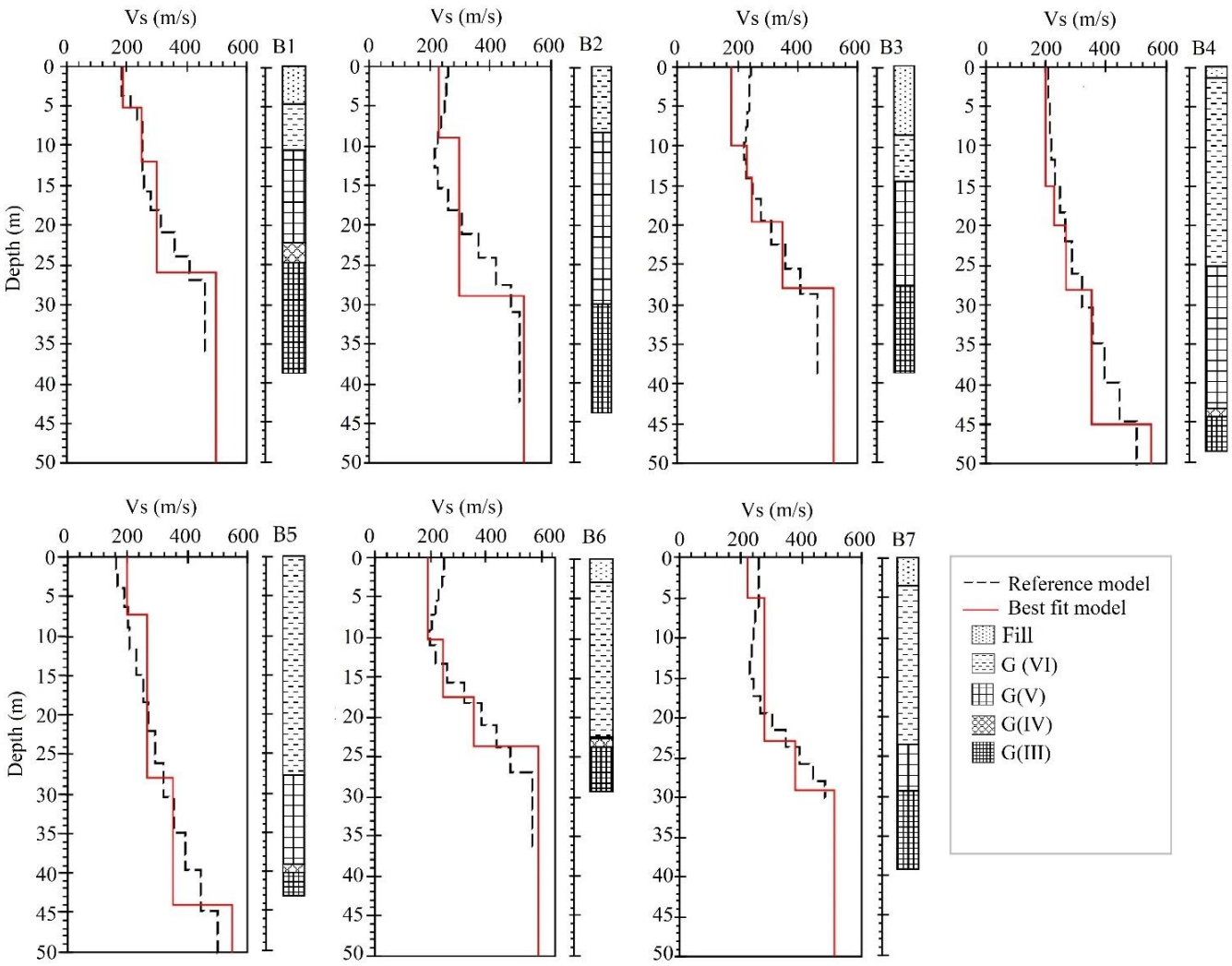

Figure 5.2. The Vs profiles generated by Rayleigh wave ellipticity from the inversion of HVSRs (red line) on boreholes near and compared to the reference model from MASW and MAM (dashed line)

soil (Vs_{30}) as an index of site's vulnerability to the earthquake and estimated via the next equation:

$$Vs_{30} = \frac{\sum_{i=1}^{n} d_i}{\sum_{i=1}^{n} (d_i / Vs_i)}$$

Where Vs_i and di are i-th layer's velocity and depth values, layers are considered only till the first 30m. For case of test sites S1 to S7, table 5.2 shows the site classification of all seven test locations according to Vs_{30} values. For site classification, the Vs_{30} in the range of 180 to 360 m/s indicates Site Class D (stiff soil). For all the sites, the site classification based on the Vs_{30} obtained by the combination of MAM and MASW and HVSR data reveal the same site class D with almost identical Vs_{30} value, which corresponds to the stiff soil class.

For site classification purposes, S-wave velocity profiles for S1-S7 were first generated following ellipticity curve inversion procedures, following by estimation of Vs30 and site classification in accordance with NEHRP recommendations. For all tested locations site classification results and comparison with the results of reference profiles can be seen in table 1. For S1-S7 sites V_{s30} lays in the range from 180 to 360 m/s, which according to [37] corresponds to the stiff soil class (Class D).

Table 5.2. Site classification results

Site ID	HVSR		Reference Vs profile	
	Vs_{30} (m/s)	Site class	Vs_{30} (m/s)	Site class
S1	280	D	275	D
S2	250	D	278	D
S3	253	D	271	D
S4	251	D	240	D
S5	252	D	228	D
S6	271	D	290	D
S7	270	D	281	D

5.4. SSR and HVSR results from earthquake data

Among the earthquakes listed in table 4.1, seismometer recordings for the highest magnitudes (4.6mb to 3.9mb) were analyzed. Unlike ambient noises, earthquake recordings have an epicenter situated quite below the surface, and spectral recordings of an earthquake is considered as more accurate data to work with. For that reason, along with SSR of Singapore territory's two seismic stations with reference to the third station, earthquake's HVSR S-wave have also been estimated for each location as shown below. Resulting earthquake HVSR data

can be seen below. Results show that fundamental frequency value for three cases were about 0.6, 1.2 and 3.4 Hz with the highest natural frequency (shallowest soft soil sediment) found in NTU territory, followed by intermediate frequency in BESC and lowest in KAPK (Figure 5.3).

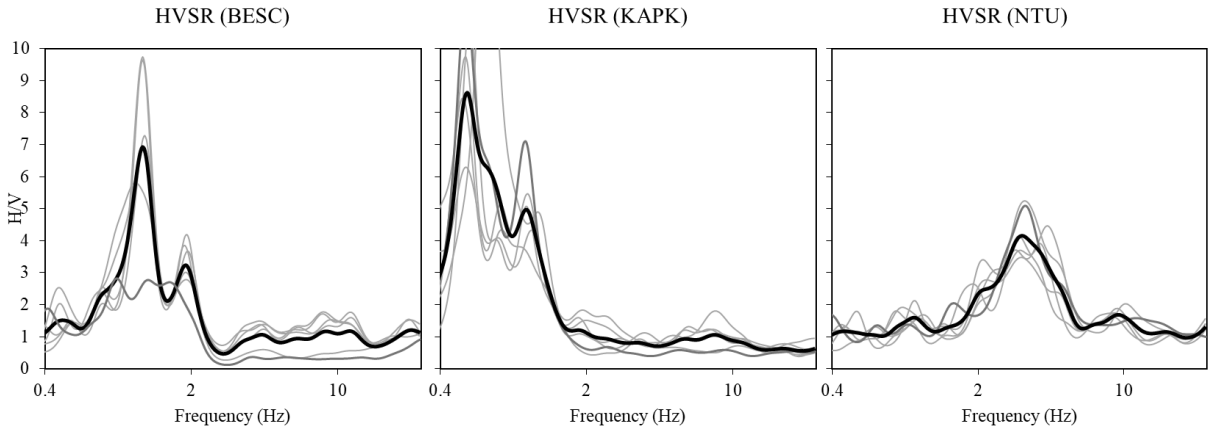

Figure 5.3. Earthquake's S-wave HVSR

Ideally, one of survey stations must be measured on outcrop, however, in case if it is not possible, conducting “relative” SSR with seismic stations with lowest bedrock depth being a reference station will still reveal site’s amplification during the same earthquake [58]. Thus, signal amplification in KAPK and BESC seismic stations will be assessed with reference to the NTU station. Subject of interest is horizontal amplification of signal in Bukit Timah Granite, horizontal SSR for both stations were measured. Figure 5.4 shows resulting amplification of sites in comparison with NTU station.

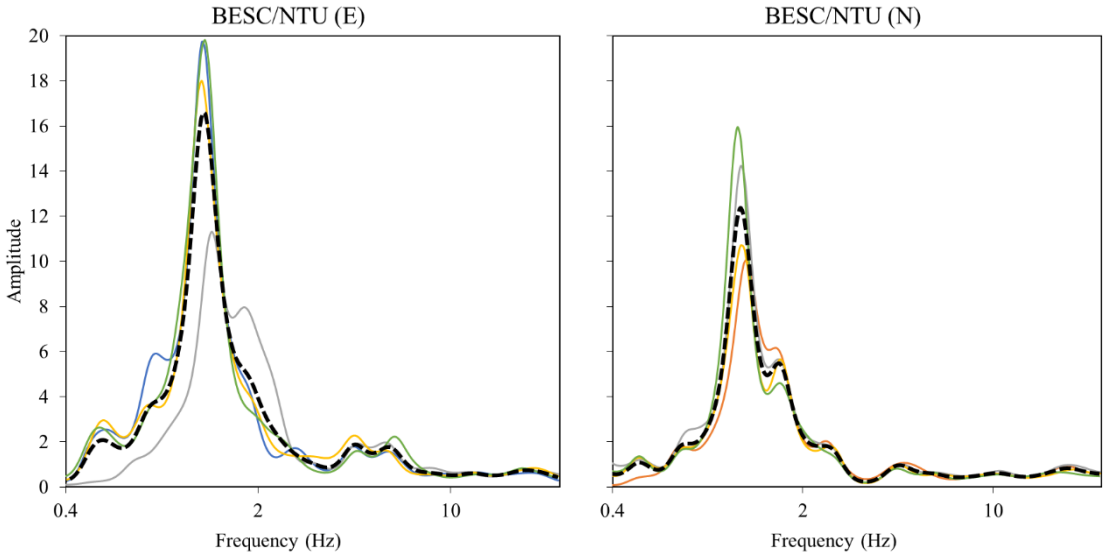

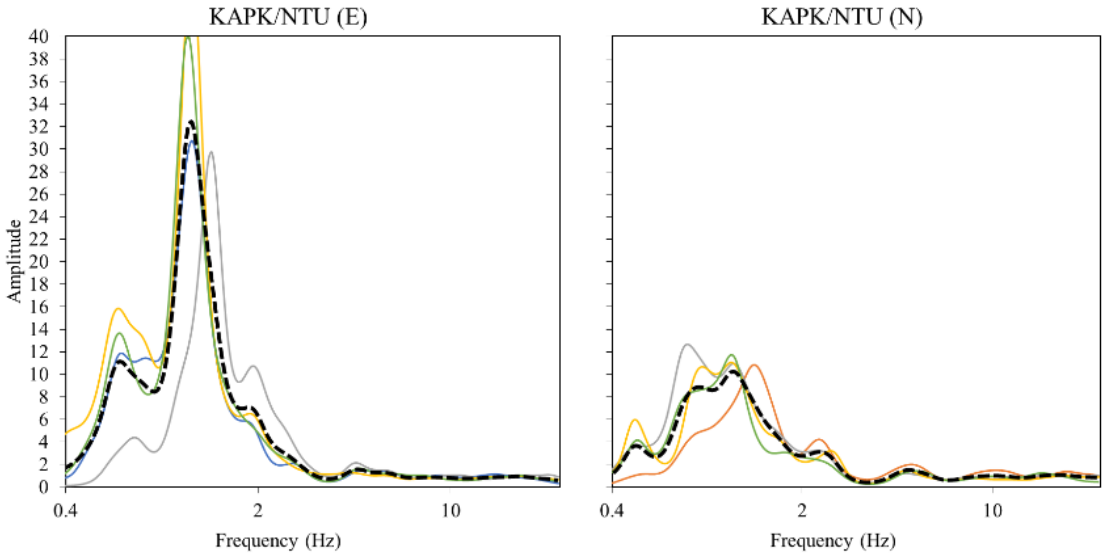

Figure 5.4. SSR of KAPK and BESC stations with reference to NTU station

BESC station is in Bukit Timah Granite and have a SSR amplitude of 16 and 13 in east and north directions. This in turn shows how soft soil layer of Bukit Timah Granite might amplify the vibration close to the fundamental frequency of the soil. SSR of seismic stations were conducted for displaying the presence of high amplitude variations in horizonal and vertical spectral amplitudes of propagated waves in Bukit Timah territory.

5.5. Numerical modelling: HVSR results

Ang Mo Kio and Marymond profiles shown in Figure 4.4 were assessed against dynamic input loads at the -500m depth. UDEC software Modeled meshes of both profiles are shown in Figure 5.5. The upper layer in the model corresponds to the soft soil sediment layer, followed by weathered granite in the middle layer and hard rock at the bottom. Layer joints are shown by green lines. Each number corresponds to the acceleration time-history results in x and y directions. Ang Mo Kio profile is considered more stable in terms of each layer depth in comparison with Marymond rd. profile. Since natural frequency of HVSR is correlated with the high impedance resistance depth (bedrock), firsly surface simulation results are compared among each other for checking the stability of the natural frequency among the models. For the Marymond rd. it is expected that natural frequencies will have higher fluctuations than in Ang Mo Kio profile.

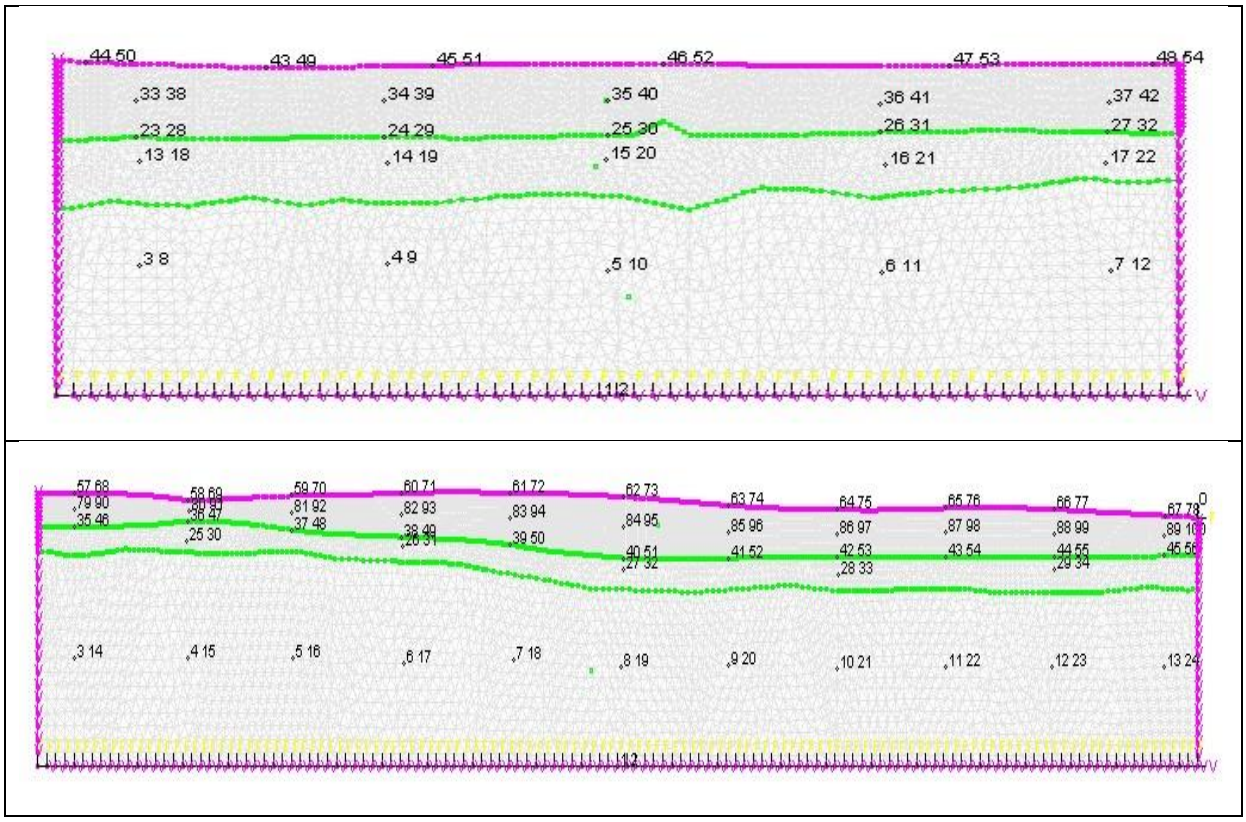

Figure 5.5. Numerical modelling generated mesh with indication of soil layers and synthetic geophones.

Resulting models reveal the same natural frequencies reveal almost no standard deviation in natural frequencies (grey bars at fundamental frequency values) between time windows for each location. Similarly, difference between natural frequencies are negligible (it varies from 3.2 to 3.4 Hz) (Figure 5.6).

Unlike the Ang Mo Kio model, for Marymond model it is expected to have a higher fluctuations in the results due to the variances in the bedrock layer depth (e.g., at point 59-58 highest frequency, and at 62-63 lowest frequency). Results of UDEC simulation can be seen from the figure 5.7 below.

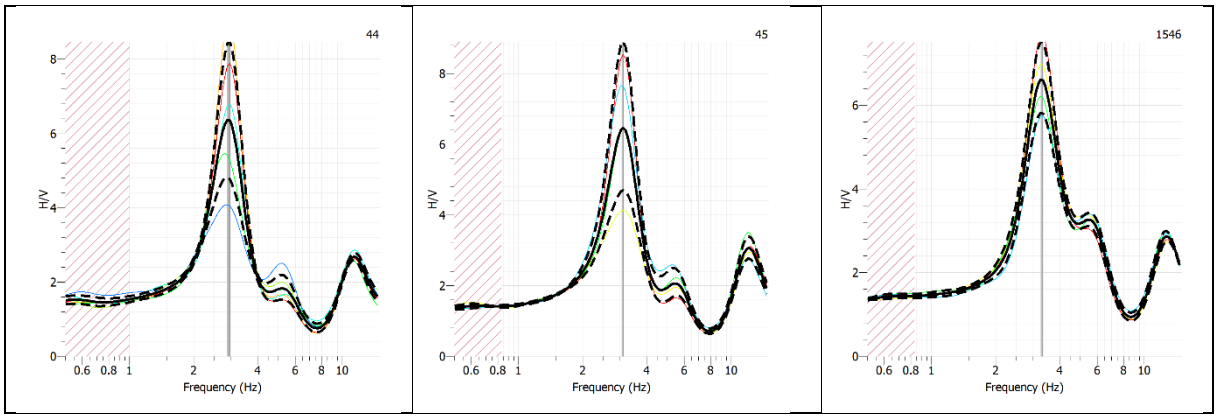

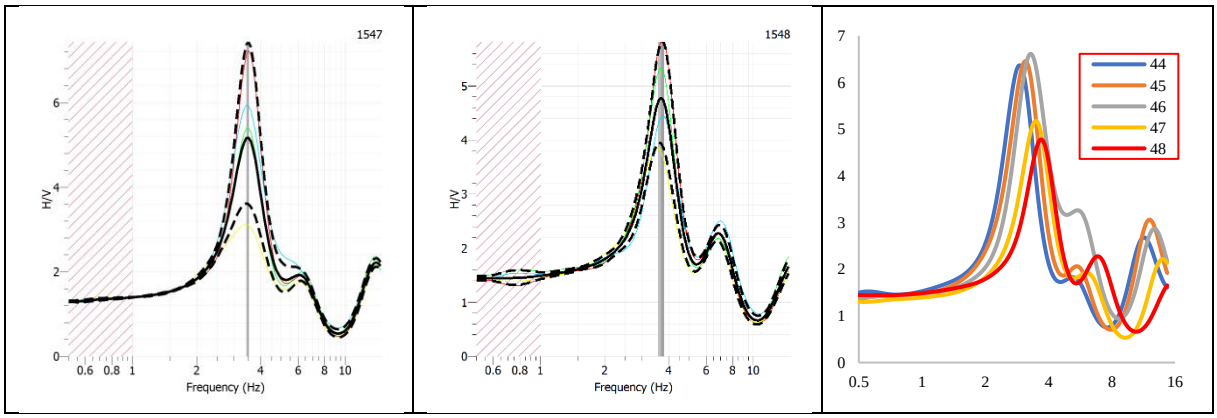

Figure 5.6. Simulation HVSR results in Ang Mo Kio for synthetic surface geophones 44-48 (1546-1548 corresponds to 46-48), and their comparison.

As it was expected from 3D Geomodel mesh, the highest frequency values (3.5-3.1 Hz) corresponded to the geophone #62 followed by #63, that had the highest soft soil sediment thickness. The shallowest sediment thickness in turn was observed geophones #57 and 58 (6.0-6.8 Hz). Conducted comparison works show that simulation calculations are constructed in a right way for recording earth vibration scenarios. Modelled soil stiffness properties were then compared with real case HVSR data as shown in figure 5.8 below. At high frequencies for both cases simulation results tend to show a peak, possibly due to the differences in model and real geology close to the surface. However, in total there is a high trend in the results between conducted site test and UDEC simulation results.

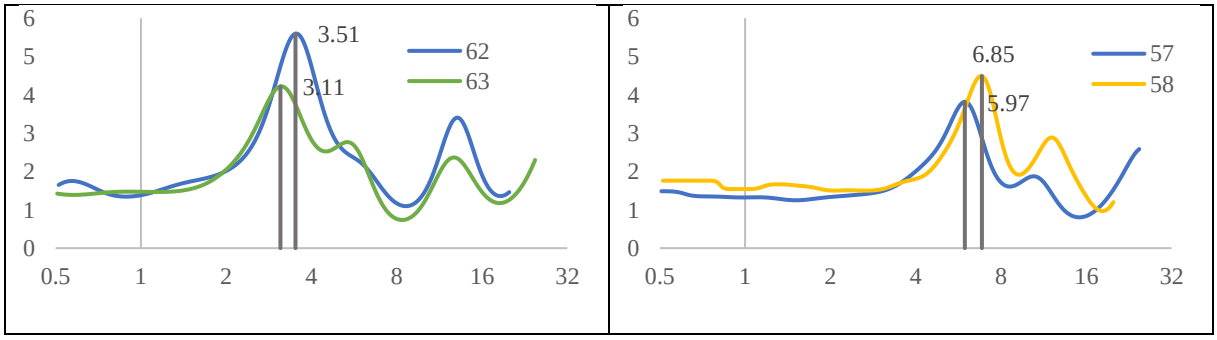

Figure 5.7. Lowest and highest natural frequencies recorded for Marymond rd model.

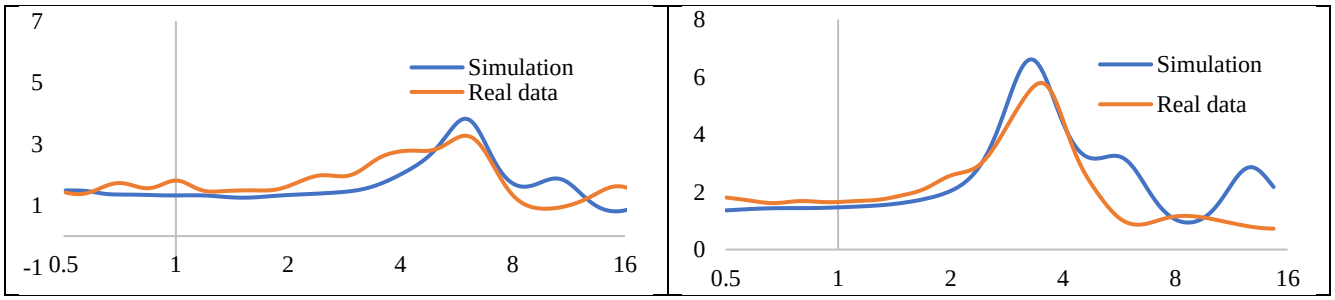

Figure 5.8. Comparison of simulation and HVSR test results in Ang Mo Kio and Marymond rd. profiles.

Conclusions

As a scope of this work, three component signals were utilized for ellipticity curve generation and its further inversion using Geopsy software. It was shown that with initial available geotechnical information, used for limitation of parameter-space size for at least uppermost soil layer, three-component signal recordings can be utilized for the site classification works. Results were compared with available geophysical site test results (MASW). This is fast and cheap alternative for estimation of dynamic soil properties with an adequate resolution. The technique is especially recommended for the zones with high urbanization levels. To broaden the methodology of ellipticity curve inversion in urban area, another type of a-priori available geotechnical or geophysical information in combined inversion or in limitation of inversion parameter space can be assessed. It was not possible to utilize HVSR data for microzonation purposes due to the unequal spacing of data over a survey area. However, in case of gathering the data with a spreading that satisfies SESAME recommendations, the methodology described in this work will be handful for seismic site microzonation.

Despite not observing direct drastic earthquake events in the Singapore territory, there are still serious tsunami and ground shaking phenomena observed. SSR of BESC seismic station implies that the Bukit Timah region witnesses high site amplification phenomena. For that reason, response of Bukit Timah region's surface to the vibratory motion is assessed using numerical modeling. 3D Geomodel of Bukit Timah Granite zone was generated based on an information gathered mostly from borehole logs, followed by geological and topological maps of the regions. Overall, more than 200 boreholes were utilized as an input data for 3D Geomodel. Model consisted of soft sediment, weathered granite and granite layers, which stiffness properties were iterated with referencing to the HVSR data of the region. 2D dynamic assessments were conducted using UDEC software and credibility of the results were assessed by 1) soft sediment layer thickness to the fundamental frequency correlation and expectations, 2) comparison of real HVSR data.

Results obtained by following described methodology is shown to be applicable for 1) site classification works, 2) site effect analysis and for mapping a synthetically generated natural frequency and HVSR amplitudes. It is believed that ellipticity curve inversion, site classification and 3D Geomodel simulation techniques described here might potentially help to improve the dynamic soil property measurements in Kazakhstan territory as well.

References

[1] Y. Nakamura, "A method for dynamic characteristics estimation of subsurface using microtremor on the ground surface," *Railway Technical Research Institute, Quarterly Reports,* vol. 30, no. 1, pp. 25-33, 1989.

[2] C. Park, R. Miller, and J. Xia, "Multichannel analysis of surface waves (MASW)," *Geophysics,* vol. 64, 05/01 1999.

[3] S. W. Moon, P. Subramaniam, Y. H. Zhang, G. Vinoth, and T. Ku, "Bedrock depth evaluation using microtremor measurement: empirical guidelines at weathered granite formation in Singapore," (in English), *Journal of Applied Geophysics,* Article vol. 171, p. 9, Dec 2019, Art. no. 103866.

[4] G. Dal Moro, "Some Aspects about Surface Wave and HVSR Analyses: a Short Overview and a Case Study," *Bollettino di Geofisica Teorica ed Applicata,* vol. 52, 06/01 2011.

[5] K. H. Stokoe and J. C. Santamarina, "Seismic-wave-based testing in geotechnical engineering," in *ISRM International Symposium,* 2000: OnePetro.

[6] S. L. Kramer, *Geotechnical earthquake engineering*. Pearson Education India, 1996.

[7] S. Yoon, *Array-based measurements of surface wave dispersion and attenuation using frequency-wavenumber analysis*. Georgia Institute of Technology, 2005.

[8] S. Foti, C. G. Lai, G. J. Rix, and C. Strobbia, *Surface wave methods for near-surface site characterization*. CRC press, 2014.

[9] B. Mi, J. Xia, J. H. Bradford, and C. Shen, "Estimating near-surface shear-wave-velocity structures via multichannel analysis of Rayleigh and love waves: An experiment at the Boise hydrogeophysical research site," *Surveys in Geophysics,* vol. 41, no. 2, pp. 323-341, 2020.

[10] E. Á. Ólafsdóttir, "Multichannel analysis of surface waves for assessing soil stiffness," University of Iceland, 2016.

[11] M. Hobiger *et al.*, "Ground structure imaging by inversions of Rayleigh wave ellipticity: Sensitivity analysis and application to European strong-motion sites," *Geophysical Journal International,* vol. 192, pp. 207-229, 01/01 2013.

[12] S.-W. Moon, Q. Khan, and T. Ku, "Application of MASW methods for investigations of shear wave velocity in residual soils of Singapore," presented at the ASCE Geotechnical and Structural Engineering Congress 2016, 2016.

[13] S.-W. Moon, P. Subramaniam, Y. Zhang, G. Vinoth, and T. Ku, "Bedrock depth evaluation using microtremor measurement: empirical guidelines at weathered granite formation in Singapore," *Journal of Applied Geophysics,* vol. 171, p. 103866, 2019/12/01/ 2019.

[14] M. Rong *et al.*, "On the Amplitude Discrepancy of HVSR and Site Amplification from Strong-Motion ObservationsOn the Amplitude Discrepancy of HVSR and Site Amplification from Strong-Motion Observations," *Bulletin of the Seismological Society of America,* vol. 107, no. 6, pp. 2873-2884, 2017.

[15] P. Gabriels, R. Snieder, and G. Nolet, "In situ measurements of shear-wave velocity in sediments with higher-mode Rayleigh waves," *Geophysical prospecting,* vol. 35, no. 2, pp. 187-196, 1987.

[16] S.-W. Moon and T. Ku, "Empirical estimation of soil unit weight and undrained shear strength from shear wave velocity measurements," in *5th International Conference on Geotechnical and Geophysical Site Characterisation, ISC 2016,* Sydney, Australia, 2016, vol. 2, pp. 1247-1252: Australian Geomechanics Society.

[17] S.-W. Moon and T. Ku, "Development of global correlation models between in situ stress-normalized shear wave velocity and soil unit weight for plastic soils," *Canadian Geotechnical Journal,* vol. 53, no. 10, pp. 1600-1611, 2016.
[18] S.-W. Moon, K. Hayashi, and T. Ku, "Estimating Spatial Variations in Bedrock Depth and Weathering Degree in Decomposed Granite from Surface Waves," *Journal of Geotechnical and Geoenvironmental Engineering,* vol. 143, 03/07 2017.
[19] S.-W. Moon and T. Ku, "Undrained shear strength in cohesive soils estimated by directional modes of in-situ shear wave velocity," *Geotechnical and Geological Engineering,* vol. 36, no. 5, pp. 2851-2868, 2018.
[20] P.-Y. Bard, "Effects of surface geology on ground motion: recent results and remaining issues," in *Proc. 10 European Conf. Earth. Eng., ed. Duma, Balkema, Rotterdam*, 1995, pp. 305-323.
[21] S. Bonnefoy-Claudet, F. Cotton, and P.-Y. Bard, "The nature of noise wavefield and its applications for site effects studies. A literature review," *Earth-Science Reviews,* vol. 79, pp. 205-227, 12/01 2006.
[22] F. Pavel and R. Vacareanu, "Investigation on site conditions for seismic stations in Romania using H/V spectral ratio," *Earthquakes and Structures,* vol. 9, no. 5, pp. 983-997, 2015.
[23] C. B. Park, R. D. Miller, J. Xia, and J. Ivanov, "Multichannel analysis of surface waves (MASW)—active and passive methods," *The leading edge,* vol. 26, no. 1, pp. 60-64, 2007.
[24] D. J. Zywicki and G. J. Rix, "Mitigation of near-field effects for seismic surface wave velocity estimation with cylindrical beamformers," *Journal of geotechnical and geoenvironmental engineering,* vol. 131, no. 8, pp. 970-977, 2005.
[25] C.-P. Lin, C.-C. Chang, and T.-S. Chang, "The use of MASW method in the assessment of soil liquefaction potential," *Soil Dynamics and Earthquake Engineering,* vol. 24, no. 9-10, pp. 689-698, 2004.
[26] N. Roy and R. S. Jakka, "Near-field effects on site characterization using MASW technique," *Soil Dynamics and Earthquake Engineering,* vol. 97, pp. 289-303, 2017.
[27] P. Subramaniam, Y. H. Zhang, Y. C. H. Ng, W. Danovan, and T. Ku, "Modal analysis of Rayleigh waves using classical MASW-MAM approach: Site investigation in a reclaimed land," (in English), *Soil Dynamics and Earthquake Engineering,* Article vol. 128, p. 11, Jan 2020, Art. no. 105902.
[28] S. Bonnefoy-Claudet, A. Köhler, C. Cornou, M. Wathelet, and P.-Y. Bard, "Effects of Love waves on microtremor H/V ratio," *Bulletin of the Seismological Society of America,* vol. 98, no. 1, pp. 288-300, 2008.
[29] D. Fäh, F. Kind, and D. Giardini, "A theoretical investigation of average H/V ratios," *Geophysical Journal International,* vol. 145, no. 2, pp. 535-549, 2001.
[30] F. Gouveia, A. Da Fonseca, R. Gomes, and P. Teves-Costa, "Deeper Vs profile constraining the dispersion curve with the ellipticity curve: A case study in Lower Tagus Valley, Portugal," *Soil Dynamics and Earthquake Engineering,* vol. 109, 06/01 2018.
[31] E. Haghshenas, P.-Y. Bard, and N. Theodulidis, "Empirical evaluation of microtremor H/V spectral ratio," *Bulletin of Earthquake Engineering,* vol. 6, no. 1, pp. 75-108, 2008.
[32] S. Parolai, S. M. Richwalski, C. Milkereit, and P. Bormann, "Assessment of the stability of H/V spectral ratios from ambient noise and comparison with earthquake data in the Cologne area (Germany)," *Tectonophysics,* vol. 390, no. 1-4, pp. 57-73, 2004.

[33] P.-Y. A. Bard, Catello, H.-B. Havenith, and S. Zacharopoulos, "Guidelines for the implementation of the H/V spectral ratio technique on ambient vibrations measurements, processing and interpretation," European Commission2004, Available: ftp://ftp.geo.uib.no/pub/seismo/SOFTWARE/SESAME/USER-GUIDELINES/SESAME-HV-User-Guidelines.pdf Accessed on: 15 January 2021.
[34] K. Konno and T. Ohmachi, "Ground-motion characteristics estimated from spectral ratio between horizontal and vertical components of microtremor," *Bulletin of the Seismological Society of America,* vol. 88, no. 1, pp. 228-241, 1998.
[35] E. Yilar, L. G. Baise, and J. E. Ebel, "Using H/V measurements to determine depth to bedrock and Vs30 in Boston, Massachusetts," *Engineering geology,* vol. 217, pp. 12-22, 2017.
[36] P. G. Malischewsky and F. Scherbaum, "Love's formula and H/V-ratio (ellipticity) of Rayleigh waves," *Wave motion,* vol. 40, no. 1, pp. 57-67, 2004.
[37] BSSC, "The 2000 NEHRP Recommended Provisions for New Buildings and Other Structures, Part I (Provisions) and Part II (Commentary)," FEMA, Washington, D.C.2001, vol. 368/369.
[38] S.-W. Moon, S. Palanidoss, Y. Zhang, V. Ganapathiraman, and T. Ku, "Bedrock depth evaluation using microtremor measurement: empirical guidelines at weathered granite formation in Singapore-NC-ND license (http:// creativecommons.org/licenses/by-nc-nd/4.0/)," *Journal of Applied Geophysics,* vol. 171, p. 103866, 10/15 2019.
[39] S. Parolai, P. Bormann, and C. Milkereit, "New relationships between Vs, thickness of sediments, and resonance frequency calculated by the H/V ratio of seismic noise for the Cologne area (Germany)," *Bulletin of the seismological society of America,* vol. 92, no. 6, pp. 2521-2527, 2002.
[40] M. Ibs-von Seht and J. Wohlenberg, "Microtremor measurements used to map thickness of soft sediments," *Bulletin of the Seismological Society of America,* vol. 89, no. 1, pp. 250-259, 1999.
[41] A. Strollo, "Development of techniques for earthquake microzonation studies in different urban environment," Universität Potsdam, 2010.
[42] K. Tokimatsu, "Geotechnical site characterization using surface Geotechnical Engineering," presented at the 1st Earthquake geotechnical engineering, Tokyo, Japan, 1995, 1997.
[43] K. TAZIME, "Minimum Group Velocity, Maximum Amplitude and Quarter Wave-length Law. LOVE-waves in Doubly Stratified Layers," *Journal of Physics of the Earth,* vol. 5, no. 1, pp. 43-50, 1957.
[44] F. Scherbaum, K.-G. Hinzen, and M. Ohrnberger, "Determination of shallow shear wave velocity profiles in the Cologne, Germany area using ambient vibrations," *Geophysical Journal International,* vol. 152, no. 3, pp. 597-612, 2003.
[45] M. Hobiger, N. Le Bihan, C. Cornou, and P.-Y. Bard, "Multicomponent signal processing for Rayleigh wave ellipticity estimation: application to seismic hazard assessment," *IEEE Signal Processing Magazine,* vol. 29, no. 3, pp. 29-39, 2012.
[46] M. Hobiger, P.-Y. Bard, C. Cornou, and N. Le Bihan, "Single station determination of Rayleigh wave ellipticity by using the random decrement technique (RayDec)," *Geophysical Research Letters,* vol. 36, p. L14303, 07/28 2009.
[47] D. Fäh, G. Stamm, and H.-B. Havenith, "Analysis of three-component ambient vibration measurements," *Geophysical Journal International,* vol. 172, pp. 199-213, 11/19 2008.
[48] M. Wathelet *et al.*, "Geopsy: A User-Friendly Open-Source Tool Set for Ambient Vibration Processing," *Seismological Research Letters,* vol. 91, pp. 1878–1889, 04/08 2020.

[49] D. Fäh *et al.*, "Using ellipticity information for site characterization," in *Network of Research Infrastructures for European Seismology*, 2009.
[50] I. Ullah, R. L. Prado, and M. Lisa, "Single-station ellipticity retrieval and its joint inversion with dispersion curve, for a borehole test site," *Arabian Journal of Geosciences,* vol. 10, no. 14, p. 316, 2017.
[51] V. Poggi, D. Fäh, J. Burjanek, and D. Giardini, "The use of Rayleigh-wave ellipticity for site-specific hazard assessment and microzonation: application to the city of Lucerne, Switzerland," *Geophysical Journal International,* vol. 188, no. 3, pp. 1154-1172, 2012.
[52] M. Wathelet, "Array recordings of ambient vibrations: surface-wave inversion," PhD, Facult´e des Sciences Appliqu´ees, Universit´e de Li`ege (Belgium), 2005.
[53] M. Sambridge, "Geophysical inversion with a neighbourhood algorithm—I. Searching a parameter space," *Geophysical journal international,* vol. 138, no. 2, pp. 479-494, 1999.
[54] Z. Tumurbaatar, H. Miura, and T. Tsamba, "Site Effect Assessment in Ulaanbaatar, Mongolia through Inversion Analysis of Microtremor H/V Spectral Ratios," *Geosciences,* vol. 9, p. 228, 05/17 2019.
[55] M. Pilz *et al.*, "First steps toward a reassessment of the seismic risk of the city of Dushanbe (Tajikistan)," *Seismological Research Letters,* vol. 84, no. 6, pp. 1026-1038, 2013.
[56] S. Ulysse, D. Boisson, C. Prépetit, and H.-B. Havenith, "Site Effect Assessment of the Gros-Morne Hill Area in Port-au-Prince, Haiti, Part A: Geophysical-Seismological Survey Results," *Geosciences,* vol. 8, no. 4, p. 142, 2018.
[57] S. Ulysse, D. Boisson, C. Prépetit, and H.-B. Havenith, "Site effect assessment of the Gros-Morne Hill area in Port-au-Prince, Haiti, Part B: Mapping and modelling results," *Geosciences,* vol. 8, no. 7, p. 233, 2018.
[58] S. Parolai *et al.*, "Site effects assessment in Bishkek (Kyrgyzstan) using earthquake and noise recording data," *Bulletin of the Seismological Society of America,* vol. 100, no. 6, pp. 3068-3082, 2010.
[59] S. Parolai, D. Bindi, and P. Augliera, "Application of the generalized inversion technique (GIT) to a microzonation study: numerical simulations and comparison with different site-estimation techniques," *Bulletin of the Seismological Society of America,* vol. 90, no. 2, pp. 286-297, 2000.
[60] A.-S. Mreyen, L. Cauchie, M. Micu, A. Onaca, and H.-B. Havenith, "Multiple geophysical investigations to characterize massive slope failure deposits: application to the Balta rockslide, Carpathians," *Geophysical Journal International,* vol. 225, no. 2, pp. 1032-1047, 2021.
[61] H.-B. Havenith, A.-S. Mreyen, A. Torgoev, and M. Micu, "Numerical models of unstable slopes in seismic areas—based on 3D geomodels," in *Workshop on World Landslide Forum*, 2017, pp. 47-57: Springer.
[62] F. Hakimov, G. Domej, A. Ischuk, K. Reicherter, L. Cauchie, and H.-B. Havenith, "Site Amplification Analysis of Dushanbe City Area, Tajikistan to Support Seismic Microzonation," *Geosciences,* vol. 11, no. 4, p. 154, 2021.
[63] P. A. Cundall, "UDEC-A Generalised Distinct Element Program for Modelling Jointed Rock," Cundall (Peter) Associates Virginia Water (England)1980.
[64] J. I. Israelsson, "Short descriptions of UDEC and 3DEC," in *Developments in geotechnical engineering*, vol. 79: Elsevier, 1996, pp. 523-528.
[65] I. s. f. s. mechanics and f. e. T. c. f. e. g. engineering, *Manual for zonation on seismic geotechnical hazards*. Japanese Society of soil mechanics and Foundation engineering, 1993.

[66] S. Mihalić, M. Oštrić, and M. Krkač, "Seismic microzonation: A review of principles and practice," *Geofizika,* vol. 28, no. 1, pp. 5-20, 2011.
[67] T. Ku *et al.*, "Practical configured microtremor array measurements (MAMs) for the geological investigation of underground space," (in English), *Underground Space,* Article vol. 6, no. 3, pp. 240-251, Jun 2021.
[68] *BS 5930: The Code of Practice for Site Investigations* (British Standards). London, England: British Standard Institution, 1999.
[69] X. H. Pan *et al.*, "Procedure for Establishing a 3D Geological Model for Singapore," in *4th GeoShanghai International Conference on Transportation Geotechnics and Pavement Engineering*, Tongji Univ, Shanghai, PEOPLES R CHINA, 2018, pp. 81-89, SINGAPORE: Springer-Verlag Singapore Pte Ltd, 2018.
[70] P.-Y. Bard, "Microtremor measurements: A tool for site effect estimation?," presented at the Second International Symposium on the Effects of Surface Geology on seismic motion, Yokohama, Japan, 1999.
[71] D. Gautam, G. Forte, and H. Rodrigues, "Site effects and associated structural damage analysis in Kathmandu Valley, Nepal. Earthq Struct 10: 1013–1032," ed, 2016.
[72] Y. Maruyama and M. Sakemoto, "Development of nationwide amplification map of response spectrum for Japan based on station correction factors," *Earthquakes and Structures*, vol. 13, no. 1, pp. 17-27, 2017.
[73] M. Zhao, Z. Gao, L. Wang, X. Du, J. Huang, and Y. Li, "Obliquely incident earthquake for soil-structure interaction in layered half space," *Earthquakes and Structures*, vol. 13, no. 6, pp. 573-588, 2017.
[74] S. Manandhar and H.-I. Cho, "New site classification system and design response spectra in Korean seismic code," 2018.